STUDY OF PION PRODUCTION FROM THE TWO-NUCLEON SYSTEM WITHIN A RELATIVISTIC UNITARY MODEL

by

Francesca Sammarruca-Machleidt

Dissertation submitted to the Faculty of the
Virginia Polytechnic Institute and State University
in partial fulfillment of the requirements for the degree of

DOCTOR OF PHILOSOPHY

in

Physics

APPROVED:

T. Mizutani, Chairman

M. Blecher

R. L. Bowden

D. A. Jenkins

C. D. Williams

September, 1988

Blacksburg, Virginia

STUDY OF PION PRODUCTION FROM THE TWO-NUCLEON SYSTEM WITHIN A RELATIVISTIC UNITARY MODEL

by

Francesca Sammarruca-Machleidt

Committee Chairman: Tetsuro Mizutani
Physics

(ABSTRACT)

In this work, we explore the $NN \rightarrow \pi NN$ reaction within a relativistic model, consistent with two- and three-body unitarity, for the NN and πNN coupled systems. The model is based on effective hadronic interactions. After describing the theoretical input, we compare the predicted NN phase parameters with the phase shift analysis. Our predictions for the $NN \rightarrow \pi NN$ spin observables are compared with the available data and with predictions from other models. A clear model dependence is observed. We also examine systematically the dependence of these spin observables on various components of the dynamical input. We identify and isolate some problems related to the present approach and we point out possible directions for future research.

Acknowledgement

First of all, it is a pleasure to thank my adviser, Tetsuro Mizutani, for his continuous interest, assistance and substantial help throughout the course of this work.

It is hard to find the words to thank my husband, Ruprecht Machleidt, for his competent help, as a physicist, and his never ending support, encouragement and patience, as a companion.

I would also like to express my deepest appreciation to Richard Silbar for enlightening discussions and most valuable advice on the manuscript.

Useful interaction with C. Fayard is gratefully acknowledged; furthermore, I would like to thank all members of the Lyon group for making their computer codes available to me.

Will and enthusiasm are not enough to succeed when the means are not available; therefore, my deepest gratitude goes to my parents, Ida and

Vincenzo Sammarruca: by taking loving care of my child during most of the time this work was performed, they actually made it possible.

My dearest friend, Chris Pirie, always available and reassuring, has helped me through the darkest moments of discouragement.

This work is dedicated to my son, Dario, with the hope that one day he will understand and forgive an always absent and busy mother.

Financial support from the U.S. Department of Energy is acknowledged.

Contents

Chapter 1

Introduction

It is the purpose of the present work to explore the $NN \rightarrow \pi NN$ reaction at intermediate energy (i. e. incident laboratory energy below 1 GeV) within the context of a relativistic meson-theoretical model consistent with two- and three-body unitarity.

This problem has recently received considerable interest, due to a rapid expansion in the experimental information available on single pion production in NN collision at intermediate energy (measurements being facilitated by the intense polarized beams at meson factories).

Parallel to this experimental progress, a growing attempt towards a unitary description of the NN system at intermediate energy has been

observed. One important driving force behind this effort has been the possibility that, in this energy range, the NN interaction may involve dibaryon resonances (structures associated with quark and gluon degrees of freedom). A rather interesting energy-dependence of spin-dependent observables has been observed experimentally [Aue+ 77] which may be related to such resonances.

However, the opening of the $N\Delta$ channel produces resonance-like structures in this energy region, such that the question arises whether the presently available data really do require an explanation in terms of quark degrees of freedom. This question cannot be answered unless conventional models of mesons interacting with baryons have been fully exploited. It must also be mentioned that quark approaches have shown, so far, a rather poor quantitative predictive power; therefore, a concrete motivation for giving up the traditional scheme in favor of a more successful one cannot be claimed.

When approaching a problem, we must ask ourselves whether some fundamental physics can be learnt from it. This is certainly the case for the πNN system : as pion production proceeds predominantly through Δ formation, one hopes to obtain useful knowledge for understanding Δ

dynamics in nuclei, which goes back to the fundamental nucleon-baryon interaction. With this objective in mind, the few-body system seems to be a very suitable choice: interesting features of the dynamics in the nuclear medium can be investigated in a 'laboratory' which is relatively simple and which allows for an exact treatment of the problem. This is the typical approach of few-body physics.

The model described in the following chapters is consistent with the one previously applied [Lam+ 87, Per 84] to the bound state reactions $NN \to NN$ and $NN \leftrightarrow \pi d$. It has been extended to incorporate the unbound $2 \to 3$ body process. We hope that the inclusion of the channel with a three-body final state will provide us with additional constraint for our theoretical input. Indeed, the $NN \leftrightarrow \pi d \leftrightarrow \pi NN$ coupled systems should be described on the same footing [AM 83] by a consistent theory, since, in the energy range considered here, they all appear to be strongly Δ-dominated.

Predictions for the $NN \to \pi NN$ reaction do exist in the literature from a few models [ML 86, Dub+ 86, DKS 87]; nevertheless, several issues make this process a still open and interesting ground for investigation. First of all, the agreement of the presently available predictions with the data is rather

qualitative; moreover, the origin of the disagreement is not fully understood. Indeed, a strong model dependence of the predictions (especially concerning the spin observables, as we will discuss in Ch. 5), together with the fact that those models have substantially different theoretical basis, leaves many questions still open.

Besides being quite different from each other in their philosophy, all existing models show some limitations: for instance, in the way the initial NN distortion is treated (the model of Kloet and Silbar [KS 80] tends to overlook the short range sector of the NN interaction), in the type of allowed intermediate states (coupled channels), and, in particular, in the way they are described (models for the Δ resonance and/or the mechanism of pion absorption and emission through the P_{11} channel).

Interestingly, the model of Kloet and Silbar [KS 80], by emphasizing the long-range part of the NN interaction, does obtain a certain degree of success in describing the bulk of the pion production data; on the other side, it has been pointed out [PSZ 87] that a realistic short-range NN potential is essential for a good description of the $NN \leftrightarrow \pi d$ data. Notice that we are looking at two equally Δ-dominated production channels (πd and πNN); these different findings indicate therefore a rather fundamental

discrepancy, which we believe should be clarified with additional study.

It is the purpose of this work to shed light on some of the problems just mentioned; in particular, we will study systematically the dependence of the πNN spin observables on the theoretical input and how they are affected by the original features of our model. As we do not attempt any phenomenological fit of the data by the introduction of ad hoc parameters, we hope to better understand the origin of the discrepancies and of the model dependence.

Unlike other works [ML 86, DKS 87], our model includes other types of πN interactions, besides the P_{11} and the (dominant) P_{33}. As pointed out in the literature [DKS 87], it would be useful to see what role the other πN channels play in this process. Moreover, our model for the P_{11} is realistic in the description of the experimental features of this partial wave; we would like to learn about the significance of this aspect for the πNN observables.

Short-range contributions are also taken into account and they include exchange of heavy bosons in the NN channel as well as in the $N\Delta$ channel.

This work is subdivided as follows: in Chapter 2 a review of the three-body formalism is given, which will set the framework for the reader. A description of the two-body interactions (major ingredient of the three-

body equation) is provided in Chapter 3. As a first test of the model, some preliminary results can be obtained from the NN channel; this will be accomplished in Chapter 4. Finally, the explicit three-body final state calculation will bring us to the analysis of the $NN \to \pi NN$ reaction (Chapter 5). Any technical aspects, in particular the numerical method developed for the solution of the three-body integral equation, will be found in the Appendices.

Chapter 2

The Formalism

2.1 Introduction

After Faddeev's formulation of the non-relativistic three-body problem [Fad 61], the theory was applied to the πNN system. It was also realized that, if the nucleon is treated as a πN pair, it is possible to include the coupling to the NN channel, which can be treated simultaneously. The non-relativistic three-body theory was then applied to πd scattering in the (3,3) resonance region.

As it is obviously very difficult to justify a non-relativistic scattering theory for pions (except of course at very low incident energies), many at-

tempts were made to incorporate relativistic kinematics or a fully relativistic pion. A relativistic three-body theory was proposed by Aaron, Amado, and Young (AAY) [AAY 68] specifically for the $\pi N - \pi\pi N$ coupled systems and later applied to πd scattering [RT 77].

In this chapter,we will describe the essential steps in the derivation of the three-body relativistic equations, and the basic assumptions necessary to set up the particular framework.

2.2 The Three-Body Equation

2.2.1 The Derivation

As a first step, one must assume a basic structure for the equation. The most widely accepted starting point for a relativistic three-body scattering theory is the Bethe-Salpeter equation (BSE) [SB 51]; even in its two-body form, the BSE is rather involved from the point of view of practical calculations, and one is faced with the necessity of making a simplifying assumption. It must be mentioned, however, that a practical simplification is not the only reason why a reduced form for the BSE is usually adopted: some problems of principle, intrinsic to the equation itself, have been found,

among which are, for instance, the interpretation of the relative time (and its consequences on the bound state problem [Nak 69]), and the lack of the correct one-body limit [Gro 82].

Furthermore, it will be assumed that the two-body sub-systems are dominated by bound states (like the deuteron), or resonances (like the P_{33}). The above is known as the 'isobar ansatz'.

As a starting point, the quasi-two-body equation for the transition matrix is assumed to have the form

$$T_{\alpha\beta}(p',p,s) = B_{\alpha\beta}(p',p,s) + \sum_{\gamma} \int \frac{d^4p''}{(2\pi)^4} B_{\alpha\gamma}(p',p'',s)\tau_{\gamma}(s,p'')T_{\gamma\beta}(p'',p,s) \tag{2.1}$$

where s is the square of the total energy in the three-body C.M. Eq. (2.1), which is shown diagramatically in Fig. 2.1, describes single particle exchange between two bound states or resonating pairs α,β and τ is the propagator of the interacting pair. The driving term B represents a single particle exchange potential (see Fig. 2.2).

The second step is to express the unitarity condition

$$S^{\dagger}S = SS^{\dagger} = \mathbf{1} \tag{2.2}$$

in terms of the solution of Eq. (2.1), using

$$S_{fi} = \delta_{fi} + (2\pi)^4 i\delta^4(p_f - p_i)T_{fi}. \tag{2.3}$$

By doing so and by allowing only two- and three-body states in the n-body phase-space element (i. e. complying with two- and three-body unitarity only), it is then possible, as shown by Aaron et al. [Aar 77], to derive expressions for the discontinuities of B and τ across the real axis (the unitarity cut).

At this point, the Blanckenbecler-Sugar (BbS) reduction consists in constructing from those discontinuities a new set of three-dimensional equations. The AAY prescription of putting the spectator particle always on its mass-shell is one possible way to achieve this purpose. A resulting delta function in the final expression for the isobar propagator, τ, allows integration over the fourth component of the momentum and, therefore, reduction of the equation to three-dimensional form.

Clearly, a certain arbitrariness has already been introduced at this stage, from which a typical 'lack of uniqueness' originates: the theory is the result of only one possible choice consistent with two- and three-body unitarity (which is directly exploited as a working tool) and the requirements of

Lorentz invariance (we discuss in the next section how the interactions, i. e. the vertices, are defined in a Lorentz invariant way).

After integration over the fourth component of the momentum, the final form of the equation is found to be [Aar 77]

$$T_{\alpha\beta}(p',p,s) = B_{\alpha\beta}(p',p,s)+\frac{1}{(2\pi)^3}\sum_{\gamma}\int \frac{d^3p''}{2E_{p''}}B_{\alpha\gamma}(p',p'',s)D_{\gamma}^{-1}(\sigma_{p''})T_{\gamma\beta}(p'',p,s) \tag{2.4}$$

where $E = \sqrt{p^2+m^2}$. Expressions for the discontinuities of B and D (the three-dimensional propagator) are obtained by directly exploiting the unitarity condition [Aar 77]. From those discontinuities, it is then possible to derive, by dispersion integral, explicit forms for B and D. Rather remarkably, what one finds for D is just the formal solution of the two-body BbS equation for the case of a separable interaction. For a system of two particles interacting in the C.M. frame via a separable potential

$$v(p',p) = \lambda g(p')g(p)\ , \tag{2.5}$$

the BbS equation reads

$$t(p',p,\sigma) = v(p',p)+\frac{1}{(2\pi)^3}\int \frac{d^3p''}{2E_1(p'')E_2(p'')}v(p',p'')\frac{E_1(p'')+E_2(p'')}{\sigma-[E_1(p'')+E_2(p'')]^2}t(p'',p,\sigma) \tag{2.6}$$

where σ is the C.M. total energy squared. The solution of Eq. (2.6) is of the form

$$t(p',p,\sigma) = g(p')D^{-1}(\sigma)g(p) \ , \tag{2.7}$$

where

$$D(\sigma) = \lambda^{-1} - \frac{1}{(2\pi)^3}\int \frac{d^3k}{2E_1(k)E_2(k)} g^2(k) \frac{E_1(k)+E_2(k)}{\sigma-(E_1(k)+E_2(k))^2} \ . \tag{2.8}$$

The same expression for D is obtained [Aar 77] following the rather lenghty derivation outlined in this section.

If the two-body system has a bound state at $\sigma = m^2$, the requirement that the D function has the appropriate pole and residue leads to the expression [AAY 68, KS 80]

$$\begin{aligned} D(\sigma) &= (\sigma-m^2)\{1-(\sigma-m^2)\frac{1}{(2\pi)^3}\int \frac{d^3k}{2E_1(k)E_2(k)} \times \\ &\quad \times g^2(k)\frac{E_1(k)+E_2(k)}{[\sigma-(E_1(k)+E_2(k))^2][m^2-(E_1(k)+E_2(k))^2]}\} \end{aligned} \tag{2.9}$$

Finally, angular momentum reduction will cast Eq. (2.4) in a convenient, one-dimensional form, amenable to practical solutions in a non-relativistic fashion.

2.2.2 The Driving Term

Following the same procedure as outlined for the propagator D, in the three-body center of mass, the explicit form for the driving term is found to be [AAY 68]

$$B_{\alpha\beta}(p', p, s) = \frac{g(\mathbf{Q}'_\alpha)(E_{\mathbf{p}'} + E_{\mathbf{p}} + \omega_{\mathbf{p}+\mathbf{p}'})g(\mathbf{Q}_\beta)}{\omega_{\mathbf{p}+\mathbf{p}'}[s - (E_{\mathbf{p}'} + E_{\mathbf{p}} + \omega_{\mathbf{p}+\mathbf{p}'})^2]} \tag{2.10}$$

where ω is the energy of the exchanged particle. The amplitude B is schematically represented in Fig. 2.2.

The vertex function g describes isobar dissociation and is therefore of crucial importance in relating the isobar (quasi-two-body) amplitude to the break-up.

In a non-relativistic theory, the arguments of the vertex functions $\mathbf{Q}'_\alpha$, $\mathbf{Q}_\beta$ are the Galilean invariant relative momenta. However, in a relativistic framework, one is faced with the problem of defining the isobar dissociation vertex (which is of course most easily expressed in the isobar C.M.) in the presence of the spectator particle, i.e. in the overall center of mass.

One source of the 'non-uniqueness' of the AAY relativistic theory lies indeed in the search for a proper definition of the relative momentum at the vertex.

It has been shown [Aar 77] that, if two particles have four-momenta k_1, k_2 in some frame (see Fig. 2.3), then the combination

$$\mathbf{Q}(k_1, k_2) = \mathbf{q} - \frac{(\mathbf{q} \cdot \mathbf{K})\mathbf{K}}{K_0(K_0 + \sqrt{K^2})} \tag{2.11}$$

where

$$q = \frac{k_1(k_2 \cdot K) - k_2(k_1 \cdot K)}{K^2} \tag{2.12}$$

and

$$K = k_1 + k_2 \tag{2.13}$$

reduces to the momentum of one of the particles in their center of mass. An analogous definition holds for the vector $\mathbf{Q}'(k_1', k_2')$ constructed with the corresponding final state variables.

It can then be shown that the quantities $|\mathbf{Q}|, |\mathbf{Q}'|, \hat{\mathbf{Q}} \cdot \hat{\mathbf{Q}}'$ are Lorentz invariant. In fact, Eq. (2.11) is the (non-unique) result of a Lorentz transformation from a system with total three-momentum $\mathbf{K}$ to a system where the total three-momentum is zero.

By using Eq. (2.11) and (2.12) to actually construct $\mathbf{Q}$, one obtains

$$\mathbf{Q} = \mathbf{p}' + \rho(p, p', z)\mathbf{p} \tag{2.14}$$

where z is the angle between $\mathbf{p}$ and $\mathbf{p}'$ and the function ρ has the form

$$\rho(p,p',z) = \sigma_{\mathbf{p}}^{-1/2}(E_{\mathbf{p}'} + \frac{\mathbf{p}\cdot\mathbf{p}'}{\sigma_{\mathbf{p}}^{1/2} + E_{\mathbf{p}'} + \omega_{\mathbf{p}+\mathbf{p}'}}) . \tag{2.15}$$

In the last expression, $p = |\mathbf{p}|, p' = |\mathbf{p}'|$ and

$$\sigma_{\mathbf{p}} = (E_{\mathbf{p}'} + \omega_{\mathbf{p}+\mathbf{p}'})^2 - \mathbf{p}^2 \tag{2.16}$$

is the invariant mass of the isobar with momentum p (see Fig. 2.2).

The above choice corresponds to the case where the exchanged particle is on its mass-shell, and is adopted in this work.

One may notice that, with the definition given in Eq. (2.14), the relative momentum is formally identical to its non-relativistic equivalent if ρ is the usual mass ratio

$$\rho = \frac{m_j}{m_j + m_k} \tag{2.17}$$

(see Fig. 2.2 for particle labels). Essentially, this means that the subsequent angular momentum projection of the B amplitudes can be done by exploiting standard non-relativistic techniques.

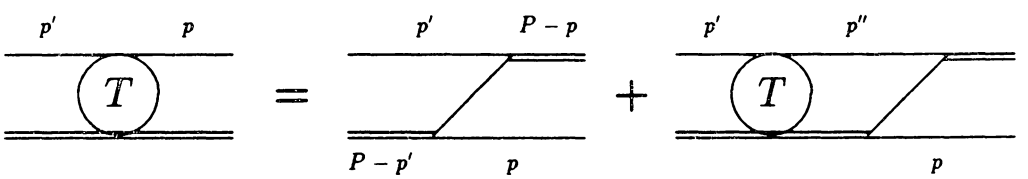

Figure 2.1: **Graphical representation of Eq. (2.1) for the scattering of a particle from a bound state or resonance (double line).**

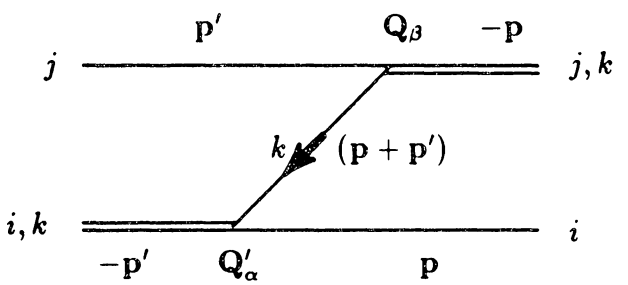

Figure 2.2: **Exchange graph for the amplitude Eq. (2.10).** α and β indicate interacting pairs. The process is: $i(j,k) \rightarrow j(i,k)$.

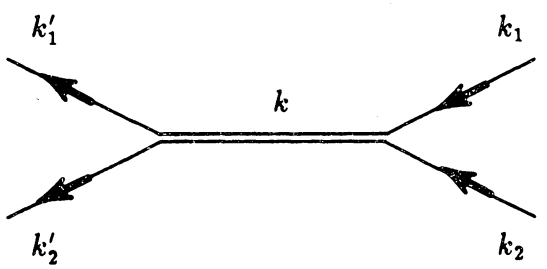

Figure 2.3: Two-body scattering through isobar formation.

Chapter 3

The Two-Body Interactions

3.1 Introduction

As stated in the previous chapter, separability is assumed to describe the two-body sub-systems, which are of two physical types: πN quasi-particle and NN correlated pair (the deuteron).

To represent the factors of the separable potential Eq. (2.5), one considers three particles (Fig. 3.1) with masses M_α ($\alpha = 1, 2, 3$), spins j_α and spin projections m_α; j and j' are the spins of the right and left isobars, respectively (we recall that the particles are assumed to bind or interact in pairs). $\mathbf{Q}$ and $\mathbf{Q}'$ are the relative momenta at the vertices, discussed in the

previous chapter.

By coupling (say, at the upper vertex) according to the scheme

$$\mathbf{j}_2 + \mathbf{j}_3 = \sigma \qquad\qquad \sigma + \mathbf{l} = \mathbf{j} \tag{3.1}$$

where $\mathbf{l}$ is the orbital angular momentum of the pair, on expansion one writes the vertex as

$$\langle \mathbf{Q} m_2 m_3 | m \rangle = \sum_{\sigma,\mu,l,\lambda} \langle j_2 j_3 m_2 m_3 | \sigma\mu \rangle \langle \sigma l \mu\lambda | jm \rangle V(Q,l,\sigma) Y_l^{\lambda}(\hat{\mathbf{Q}}) \tag{3.2}$$

with V the form factor.

In the following sections, the choice of the vertex functions and their parametrizations will be discussed, with particular emphasis on the P_{33} channel, becouse of its dominant role in controlling the inelasticity in this energy range.

3.2 The P_{33} Channel

The P_{33} channel (i. e. a πN pair interacting through a P_{33} partial wave) is by all means the most important channel in the energy range under consideration and in particular for our purposes, as pion production proceeds predominantly through Δ excitation.

Given the dominant role of this partial wave, one can raise the question whether or not the separability assumption is realistic. It has been shown by Reiner [Rei 84] that the P_{33} is separable up to a very high degree of accuracy (we will come back to this point later in the section). However, when working in a potential-theoretic (rather than field-theoretic) approach, one must keep in mind the following: the on-shell information from $\pi - N$ scattering does not uniquely determine the off-shell behaviour of the amplitude. Some care must then be exercised in the choice of the off-shell form factors (which contain all the dynamical off-shell dependence), rather than simply extrapolating in an ad hoc manner from the on-shell information.

We recall that the P_{33} scattering matrix, on- and off-shell, is written as

$$t(p', p, \sigma) = v(p')D^{-1}(\sigma)v(p) \tag{3.3}$$

where

$$D^{-1}(\sigma) = \frac{1}{\sigma - M_\Delta^2 - I(\sigma)} \tag{3.4}$$

(σ is the C.M. total energy squared). In the last equation, $I(\sigma)$ is the integral appearing in Eq. (2.8). M_Δ, the bare Δ mass, is taken to be 1320 MeV [WMA 75].

The parameters of the form factor, which is chosen, for the on-shell case,

as

$$v(p) = \frac{\alpha p}{p^2 + \beta^2} \tag{3.5}$$

are then constrained by the $\pi N - P_{33}$ scattering data. A satisfactory fit of the P_{33} phase shifts is obtained with $\alpha = 218.58$ fm^{-1}, $\beta^2 = 2.17$ fm^{-2}.

However, when the form factor Eq. (3.5) is used for 'off-shell' $\pi - N$ scattering, the applied cutoff turns out to be too strong (i.e. the associated range too long), which naturally results in a substantial underestimation of pion production.

As a remedy to this problem various prescriptions are available from theories of off-shell continuation of the πN scattering matrix. One way, already used in $NN \rightarrow \pi d$ calculations [Lam+ 87], consists in defining a new form factor

$$F(p) = v(k)\frac{h(p)}{h(k)} \tag{3.6}$$

where k is the center of mass momentum for on-shell $\pi - N$ scattering, defined by

$$\sigma = (\sqrt{m^2 + k^2} + \sqrt{\mu^2 + k^2})^2 \tag{3.7}$$

and $h(p)$ a new form factor to be chosen. The ratio in Eq. (3.6) mantains the on-shell behaviour, as given in Eq. (3.5).

Even in the simple case of a monopole form for $h(p)$

$$h(p) = \frac{k^2 + \lambda_{33}^2}{p^2 + \lambda_{33}^2} \tag{3.8}$$

the choice of the cutoff mass λ_{33} is rather delicate; this is essentially a free parameter (within some latitude, as explained later), and one must establish some criteria to constrain it.

Naturally, we expect the P_{33} off-shell behaviour to effect mostly those NN waves which couple to a very central $N\Delta$ state, for instance ${}^1D_2$ and ${}^3F_3$, which contribute to the inelasticity through the transitions ${}^1D_2 \rightarrow {}^5S_2$ and ${}^3F_3 \rightarrow {}^5P_3$. In fact, one could argue that the ${}^3F_3$ NN partial wave is a good ground to test and constrain the off-shell P_{33} potential: because of its rather peripheral nature, it should not be drastically effected by short-range contributions. Also, only the Δ can control the inelasticity, since no other πN resonance has its threshold within this energy range.

Exploiting the off-shell freedom until good ${}^3F_3$ NN phase parameters are achieved seems of course very attractive; things are however more complicated as other partial waves must also be kept in mind. To fit the more central ones, for instance the P waves, requires a very careful choice of both P_{33} and P_{11} off-shell amplitudes. This cannot be done by only looking at

the $^3F_3$ inelasticity.

A recent study in this direction [Ued 86a] seems to indicate a large off-shell freedom of the P_{33} and a rather remarkable effect on the $^3F_3$ phase parameters. From this, it is claimed, one could easily constrain the off-shell potential. Unfortunately, other partial waves do not remain stable under changes in the P_{33} off-shell behavior, and a different choice of a rank-one separable potential or off-shell parameters does not appear to offer a simple solution.

This is seen in Fig. 3.2, where we show the the sensitivity of the $^3F_3$ phase parameters to the cutoff mass of the off-shell form factor, λ_{33}, within the pole-resonance model of Eq. (3.6). It is rather obvious that a gain in inelasticity implies too much attraction in the real part of the phase shifts; this undesirable behaviour will of course manifest itself in other partial waves as well, and therefore is not a possible solution.

Some comments are due, here, concerning what establishes an acceptable range of the cutoff, in relation to the underlying physics of the off-shell $\pi N - P_{33}$ system. It was shown [Rei 84] that the model of Eq. (3.6), with a cutoff of about 700 MeV, can very well 'simulate' the behaviour of the half-off-shell (either the final or the initial particles are off-shell) P_{33} scatter-

ing matrix as calculated from off-shell continuation in a dispersion relation approach. This comparison was in fact designed as a 'separability test', meant to assess the validity of potential-theoretic approaches and to help constrain the off-shell behaviour. At this point, one would hope to have gained some insight into the dynamical content of the P_{33}; however, as we have seen, when inserted in the NN calculation, the model is obviously insufficient.

Interestingly, the problem of the poor ${}^3F_3$ inelasticity is shared by other models. It is well known that, even though meson theory can provide a very quantitative description of the low energy NN data [Lac+ 80, MHE 87], things become rather qualitative above pion production threshold (which shows how poorly inelasticities are still understood). In relation to our discussion on the P_{33} off-shell effects, it is quite interesting to compare with a field-theoretic approach, as not so much off-shell freedom is left in such a framework. The result of this comparison is shown in Fig. 3.3, where the dash-dot curve [Mac 88] is obtained from the extension above pion production threshold of the Bonn meson-exchange model for the NN interaction. The dotted curve is from a similar model, but with a static meson propagator [Mac 88]. (The static limit approximation does, indeed,

have a non-negligible effect, especially on $^3F_3$.)

It is difficult not to ask ourselves whether some fundamental physics may be missing here. It appears, so far, that a field theory of mesons and baryons cannot simultaneously and correctly describe both the NN and the πN sectors, even though the same fundamental vertices are involved. Describing one or the other is really a matter of choice and depends on one's priorities. (The study of the P_{11} channel, in the next section, should provide support for this statement.)

On the other side, we feel that the model used in the present work has not yet reached a sufficient degree of sophistication. In fact, a model for the off-shell behavior designed to improve the NN inelasticities is currently under investigation [MF 88]. However, even if better inelasticities are achieved, we should keep in mind that the above questions must still be answered.

In the present work we have obtained pion production predictions within the standard P_{33} model, Eq. (3.6), performing, however, a study of the off-shell parameters in relation to the pion production differential cross-section (as shown in a later chapter). In fact, in spite of obvious discrepancies, it may still be rather interesting to examine various production channels on

the same footing, which is our objective, as this may help in locating and further restricting possible causes of problems.

3.3 The P_{11} Channel

Even though pion production through the P_{33} channel is by far the dominant mechanism, various features make the P_{11} πN interaction rather interesting.

First of all, there is its unique behaviour: the phase shifts are small and negative at low energy, then change sign and start rising very rapidly at about 170 MeV.

The scattering amplitude has a pole at $\sigma = m^2$, which is due to the coupling of the pion and the nucleon with the positive energy nucleon.

A microscopic theory able to explain the above features from fundamental πN scattering principles is presently not available. It is well known that a scattering amplitude, with a dynamically generated nucleon pole [KS 80], as obtained, for instance, from Eqs. (2.6-9), cannot even qualitatively reproduce the experimental behaviour of the P_{11}.

It was already realized [Miz+ 81, BA 81] that, in order to reproduce

the sign change of the phase shifts, it is necessary to introduce at least another channel. In addition, one must generate the nucleon pole to take into account the effect of pion absorption and emission through the P_{11} channel.

The model we use was first developed [Miz+ 81] in the light of the previous considerations. One writes the total amplitude as a sum of two contributions

$$t = t_P + t_{NP} \tag{3.9}$$

the 'pole' and the 'non-pole' part, where

$$t_{NP}(p', p, \sigma) = g_{NP}(p') D_{NP}^{-1}(\sigma) g_{NP}(p) \tag{3.10}$$

and

$$t_P(p', p, \sigma) = g_P(p', \sigma) D_P^{-1}(\sigma) g_P(p, \sigma) \tag{3.11}$$

with the propagators D_{NP}^{-1}, D_P^{-1} as in Eq. (2.8), (2.9) respectively.

The energy-dependent vertex function $g_P(p, \sigma)$ (notice the different dependence in the case of the non-pole term) was obtained by 'dressing' the πNN vertex and the nucleon propagator to take radiative corrections into

account [Miz+ 81], and has the form

$$g_P(p,\sigma) = f(p,\sigma) + \frac{1}{(2\pi)^3}\int_0^\infty \frac{k^2 dk}{2E_k\omega_k} f(k,\sigma)\frac{E_k+\omega_k}{\sigma-(E_k+\omega_k)^2} t_{NP}(k,p,\sigma) \tag{3.12}$$

with

$$f(p,\sigma) = (\frac{24\pi m}{E_p+m})^{1/2} G \frac{p}{p^2+\gamma^2} \tag{3.13}$$

G is the (dimensionless) πNN coupling constant ($= 13.4$) and $\gamma = 5.5$ fm^{-1}. For the non-pole part, we choose the form factor [Miz+ 81]

$$g_{NP}(p) = \frac{\alpha p}{p^2+\beta^2} \tag{3.14}$$

with $\alpha = 182.58$ fm^{-1} and $\beta^2 = 13.50$ fm^{-2}.

Off-shell modifications are performed in a similar fashion as in Eq. (3.6), and a monopole form is adopted for the off-shell form factor. The choice of its cutoff mass, as usual, poses some questions. A value of 1.2 GeV has been traditionally adopted [Lam+ 87] in πd calculations for both the pole and the non-pole parts; however, it was then realized that, when the πNN vertex receives contributions from the non-pole part, the effective cutoff is actually much stronger (about 700 MeV). This has resulted in an undesirably large attraction, particularly in the NN P-waves, an effect which is enhanced as the energy increases. In Fig. 3.4 we show the sensitivity of the $^3P_1$ partial

wave to the parametrization of the $\pi N - P_{11}$ vertex. We must mention that short-range forces (heavy boson exchanges in the NN sector) are not included in any of the curves appearing in this chapter, as the objective is to isolate off-shell effects and/or sensitivity to different treatments of the πN system. Nevertheless, even their inclusion cannot totally eliminate the large discrepancy observed in the figure (solid curve in particular). One can see that, by simply increasing the strength (or weakening the cutoff) of the pole term as compared to the non-pole, a substantial reduction of the attraction can be achieved. In fact, the problem can in principle be partially cured by adopting a rank-one potential and adjusting the off-shell parameters on the NN data as much as possible (as is actually done in standard NN models).

A correct description of the P_{11} would, however, be no longer possible. Again, the issue of the simultaneous description of the NN and the πN problems (already mentioned in the previous section) comes up clearly. The off-shell nature of the P_{11} is also being presently investigated from the point of view of πd elastic scattering, a process which is known to be rather sensitive to the description of this πN partial wave (and much less to P_{33} off-shell effects). On the other hand, the pion production mechanism may

not be the best ground to detect dramatic effects due to differences in the P_{11} input, because of the clear dominance of the P_{33}.

3.4 The 'Small' πN Waves

Following previous work by Lamot and collaborators [Lam+ 87], the following form factor is chosen for the S_{11}, S_{31}, P_{13} and P_{31}:

$$g_l(p) = p^l[\frac{A}{p^2+a^2} + \frac{B}{p^2+b^2}] \tag{3.15}$$

The parametrizations [SZM 79] adopted for each wave are given in Table 3.1. They are fitted to the phase shifts and the scattering volumes.

3.5 The Deuteron

For the NN two-body interactions, we retain the ${}^3S_1 - {}^3D_1$ coupled channels. The form factors are of the type [Per 84, Lam+ 87]

$$g_l(p) = p^l \frac{1 + a_l p^2}{\prod_{i=1}^{l+2}(1 + b_{li} p^2)} \tag{3.16}$$

The parametrizations, chosen to reproduce the ${}^3S_1$ phase shift, and the deuteron binding energy, quadrupole moment, charge form factor and $D-$state

probability (6.7%) are given in Table 3.2.

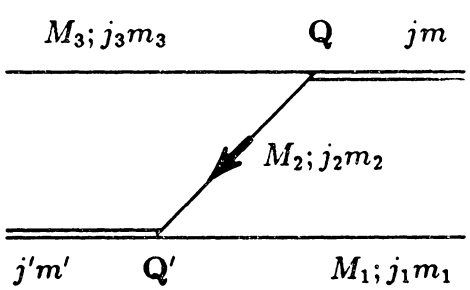

Figure 3.1: **Mass and spin labelling for the exchange-graph Fig. 2.2.**

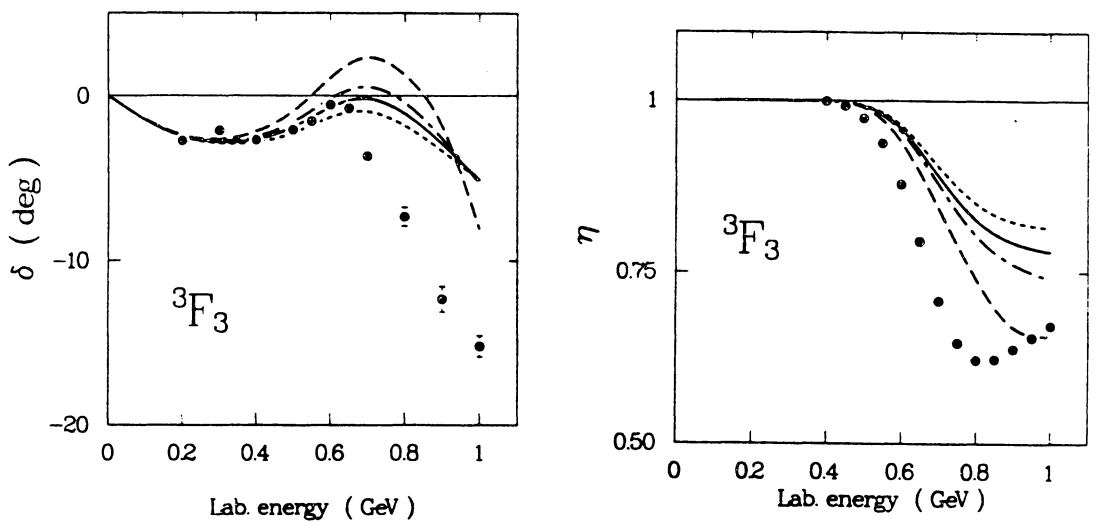

Figure 3.2: **Variation of the $^3F_3$ phase parameters with the cutoff mass of the off-shell $\pi N - P_{33}$ vertex.** $\lambda_{33} = 0.7$ GeV (dotted), $\lambda_{33} = 0.8$ GeV (solid), $\lambda_{33} = 0.9$ GeV (dash-dot), $\lambda_{33} = 1.2$ GeV (dashed). Data from Arndt et al. [Arn+ 83].

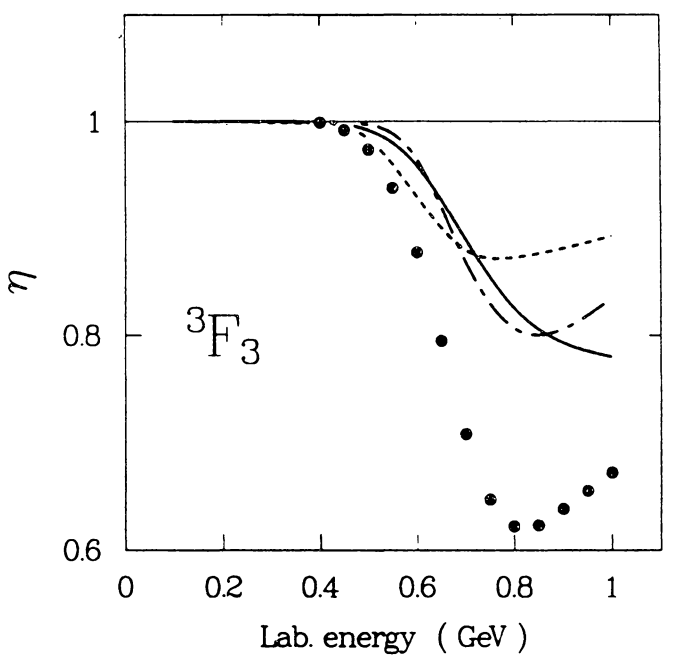

Figure 3.3: $^3F_3$ inelasticity as from our model with $\lambda_{33} = 0.8$ GeV (solid) and from two field-theoretic models (dotted and dash-dot) [Mac 88].

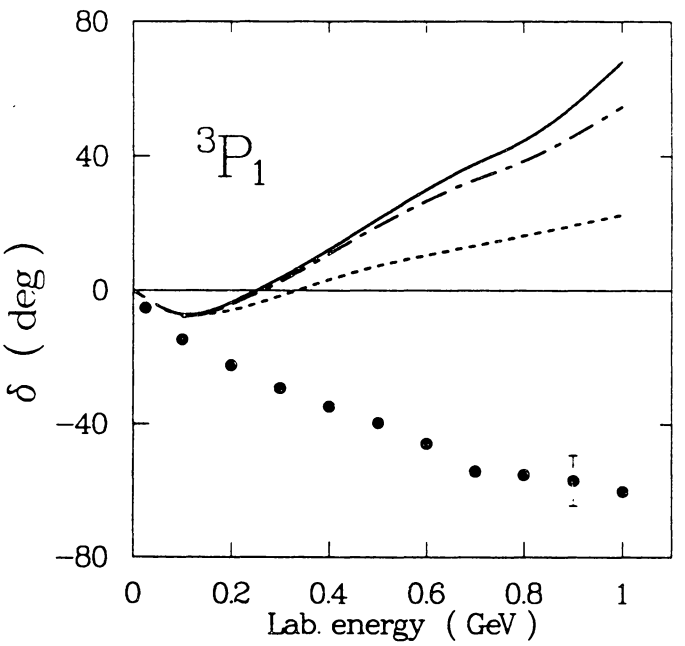

Figure 3.4: **Sensitivity of the $^3P_1$ to the parametrization of the $\pi N - P_{11}$ vertex.** Solid line: rank-two P_{11} with a cutoff of 1.2 GeV for the pole and non-pole part; dash-dot line: 1.5 GeV for the pole and 1 GeV for the non-pole; dotted line: pole only with 1.5 GeV. Data from [Arn+ 83].

Table 3.1: **Parameters for the "small" πN waves.**

	A (fm^{-2})	a^2 (fm^{-2})	B (fm^{-2})	b^2 (fm^{-2})
S_{11}	262.82	14.76	0.00	—
S_{31}	1660.09	36.49	−26.95	1.19
P_{13}	97.25	6.97	−81.14	16.98
P_{31}	111.19	6.82	0.00	—

Table 3.2: **Parameters for the deuteron.**

l	a_l	i	b_{li}
0	−0.038	1	0.351
		2	0.190
2	0.34	1	0.0217
		2	0.428
		3	0.384
		4	0.079

Chapter 4

The NN Channel

4.1 Introduction

Since the mid $70's$, considerable experimental effort has been spent at meson factories to measure elastic and inelastic NN scattering systematically up to 1 GeV.

Presently, our theoretical understanding of the inelasticities is by no means complete, as should be clear from the previous chapter. It is enough to mention that new (unobserved) phenomena, like baryon-baryon resonances, have been suggested to explain the rich spin structure of the NN system above the inelastic treshold.

The most important 'conventional' source of inelasticity in the energy regime under consideration is the $NN \rightarrow N\Delta$ treshold at 600 MeV. Because of isospin conservation, it can occur in $T = 1$ two-nucleon states only. (Double Δ excitation, possible for both isospin zero and one states, has its threshold above 1 GeV.)

During the past decade, speculations on the possible existence of dibaryon resonances have blossomed considerably, but at present there is no firm evidence for such exotic states. Rather interesting energy-dependent structures have been found experimentally, among which are the by now well-measured spin-dependent total cross section differences

$$\Delta\sigma_T^{tot} = \sigma^{tot}(\uparrow\uparrow) - \sigma^{tot}(\uparrow\downarrow) \tag{4.1}$$

$$\Delta\sigma_L^{tot} = \sigma^{tot}(\rightrightarrows) - \sigma^{tot}(\rightleftarrows) \,. \tag{4.2}$$

Hidaka et al. [Hid+ 77] proposed that the peaks around 550 MeV in these quantities could be due to a ${}^1D_2$ resonance, and the inverted peak in $\Delta\sigma_L^{tot}$ around 800 MeV to a ${}^3F_3$ resonance. Indeed, phase shifts analysis of elastic data do reveal resonance-like half-loops in the Argand diagrams for the ${}^1D_2$ and ${}^3F_3$ amplitudes [KTS 81].

However, the presence of a loop in the Argand plot by itself is a necessary but not sufficient condition for the existence of a resonance: the opening of the $N\Delta$ channel in the same region produces, at least qualitatively, the observed resonance-like structures, leading to half-loop behaviors in the controversial waves. In the study of Kloet et al. [KTS 81], strong indications have been found that such a behavior is not due to a resonance pole but to the coupling with the inelastic πNN channel.

Theoretical models [KS 81, Lom 82, Lee 84, PSZ 87, Mac 88] explain the total cross section differences up to the degree of quality to which they reproduce the phase shift analysis, especially in the two critical partial waves. In fact, (as already mentioned in Ch. 3), this is where almost all models share common deficiencies. Generally, all πNN theories tend to underestimate the $^1D_2$ inelasticity above the $N\Delta$ threshold; the early model of Kloet and Silbar [KS 80] does, however, substantially overestimate it, which is probably due to a very strong coupling to the $^5S_2$ $N\Delta$ channel mostly through the tensor part of the pion exchange force. (This point will be further discussed in Ch. 5.)

As far as $^3F_3$ is concerned, the real phase shifts don't show enough attraction around 650 MeV and enough repulsion above 700 MeV, while

the inelasticity is insufficient just about everywhere.

For most πNN theories, it is especially difficult to reproduce quantitatively phase shifts analysis results for the P-waves, typically showing insufficient repulsion above 500 MeV in $^3P_1$ and $^3P_0$. The behaviour of these waves in the inelastic region is characterized by the fact that the coupled $N\Delta$ channels are also in a relative P wave, so that the NN and $N\Delta$ states should contribute in an equally important way. This is not the case for $^1S_0$, which couples to a $N\Delta$-wave in a relative $D-$state, and where exchanges in the short range NN sector do play the essential role.

It is known that one must quantitatively account for the S and P waves in order to reproduce elastic NN observables. (As we shall discuss in a later chapter, this does not apply so strictly to the inelastic observables).

Ideally, one would like to describe equally well elastic and inelastic processes, but this turns out to be a very difficult task and has not yet been achieved. The most sophisticated NN models [MHE 87] which rather carefully describe the low energy NN data, don't do much better above the threshold than potential theoretic approaches (see Ch. 3). Presently, it is not clear if this is an indication of the the limitations of meson models or simply is due to the fact that the models for higher energy have not yet

been worked out as carefully as for the low-energy regime. For the time being, it may be more conservative to suspect the second option.

4.2 The One-Boson-Exchange Amplitudes

In this section, we discuss how short-range forces are included in our model. As previously explained (Ch. 2), the three-body equation generates isobar amplitudes on iteration of the one-pion-exchange driving terms, which represent the long-range part of the nuclear force. Any other contribution (potential) is independently evaluated and added to the driving terms.

The short-range contribution to the NN interaction comes primarily from the ω, ρ and σ bosons (the η, δ and ϕ mesons play only a small role), the σ being a fictitious scalar isoscalar particle introduced to account for the attractive intermediate range part of the NN potential. The σ can be understood as an approximate representation of two correlated pions in relative S-wave and is in general assumed to have a mass between 500 and 600 MeV. The following properties are attributed to those mesons, from experimental studies of two- and three-pion resonances [PDG 84]:

vector ρ: $J^\pi = 1^-, T = 1, m_\rho \approx 770$ MeV, $\Gamma_\rho \approx 150$ MeV

vector ω: $J^\pi = 1^-, T = 0, m_\omega \approx 780$ MeV, $\Gamma_\omega \approx 10$ MeV

vector ϕ: $J^\pi = 1^-, T = 0, m_\phi \approx 1020$ MeV, $\Gamma_\phi \approx 4$ MeV

pseudoscalar η: $J^\pi = 0^-, T = 0, m_\eta \approx 550$ MeV, $\Gamma_\eta \approx 0$ MeV

scalar δ: $J^\pi = 0^+, T = 1, m_\delta \approx 980$ MeV, $\Gamma_\delta \approx 50$ MeV

where T denotes the isospin and Γ_α the full width.

The interaction Lagrangians for meson-nucleon couplings are

$$\mathcal{L}_{ps} = -g_{ps}\bar{\psi}i\gamma^5\psi\varphi_{ps} \tag{4.3}$$

$$\mathcal{L}_{s} = +g_{s}\bar{\psi}\psi\varphi_{s} \tag{4.4}$$

$$\mathcal{L}_{v} = -g_{v}\bar{\psi}\gamma_\mu\psi\varphi_v^\mu - \frac{f_v}{4M}\bar{\psi}\sigma_{\mu\nu}\psi(\partial^\mu\varphi_v^\nu - \partial^\nu\varphi_v^\mu) \tag{4.5}$$

with ψ the nucleon and φ_α the meson fields. For isospin 1 mesons φ_α is to be replaced by $\tau \cdot \varphi_\alpha$ with τ_i the usual Pauli matrices. ps, s, and v denote pseudoscalar, scalar, and vector coupling/field, respectively.

The one-boson-exchange potential (OBEP) is defined as a sum of one-particle-exchange amplitudes of certain bosons with given mass and coupling. Thus,

$$V_{OBEP} = \sum_{\alpha=\eta,\rho,\omega,\delta,\sigma} V_\alpha^{OBE} \tag{4.6}$$

which is then added to the one-pion-exchange amplitude. (The contributions from the iso-vector bosons δ and ρ are to be multiplied by a factor

$\tau_1 \cdot \tau_2$.)

The above Lagrangians lead to the following OBE amplitudes (see Fig. 4.1 for particles labels):

$$\begin{aligned}
\langle \mathbf{q}'\lambda_1'\lambda_2'|V_{ps}^{OBE}|\mathbf{q}\lambda_1\lambda_2\rangle &= g_{ps}^2\bar{u}(\mathbf{q}',\lambda_1')i\gamma^5 u(\mathbf{q},\lambda_1)\bar{u}(-\mathbf{q}',\lambda_2')i\gamma^5 u(-\mathbf{q},\lambda_2) \\
&\quad /[k^2 - m_{ps}^2] \qquad (4.7) \\
\langle \mathbf{q}'\lambda_1'\lambda_2'|V_s^{OBE}|\mathbf{q}\lambda_1\lambda_2\rangle &= g_s^2\bar{u}(\mathbf{q}',\lambda_1')u(\mathbf{q},\lambda_1)\bar{u}(-\mathbf{q}',\lambda_2')u(-\mathbf{q},\lambda_2) \\
&\quad /[k^2 - m_s^2] \qquad (4.8) \\
\langle \mathbf{q}'\lambda_1'\lambda_2'|V_v^{OBE}|\mathbf{q}\lambda_1\lambda_2\rangle &= \{g_v\bar{u}(\mathbf{q}',\lambda_1')\gamma_\mu u(\mathbf{q},\lambda_1) \\
&\quad + \frac{f_v}{2M}\bar{u}(\mathbf{q}',\lambda_1')\sigma_{\mu\nu}i(q'-q)^\nu u(\mathbf{q},\lambda_1)\} \\
&\quad \times\{g_v\bar{u}(-\mathbf{q}',\lambda_2')\gamma^\mu u(-\mathbf{q},\lambda_2) \\
&\quad - \frac{f_v}{2M}\bar{u}(-\mathbf{q}',\lambda_2')\sigma^{\mu\nu}i(q'-q)_\nu u(-\mathbf{q},\lambda_2)\} \\
&\quad /[k^2 - m_v^2] \qquad (4.9)
\end{aligned}$$

where λ_i (λ_i') denotes the helicity of an incoming (outgoing) nucleon which is defined as the eigenvalue of the operator $\mathbf{s}\cdot\hat{\mathbf{q}}$, with $\mathbf{s}$ the spin operator and $\hat{\mathbf{q}} = \mathbf{q}/|\mathbf{q}|$ the unit momentum operator of the respective nucleon. Also, $E = \sqrt{M^2 + \mathbf{q}^2}$ and $E' = \sqrt{M^2 + \mathbf{q}'^2}$ while k is the four-momentum transfer.

Dirac spinors are normalized such that $\bar{u}(\mathbf{q},\lambda)u(\mathbf{q},\lambda) = 2M$ with $\bar{u} =$

$u^\dagger\gamma^0$. In the propagator for vector bosons,

$$\frac{-g_{\mu\nu} + k_\mu k_\nu / m_v^2}{k^2 - m_v^2} , \tag{4.10}$$

we have dropped the $k_\mu k_\nu$-term, which vanishes on-shell. (The off-shell effect of this term was examined by Holinde and Machleidt [HM 75] and was found to be unimportant.)

After carrying out the Dirac algebra, the helicity amplitudes are expressed in the coupled $|LSJ\rangle$ basis, to be made compatible with the three-body calculation. This is done by using the partial wave expansion of the helicity amplitude,

$$\langle \mathbf{q}'\lambda_1'\lambda_2'|V_\alpha|\mathbf{q}\lambda_1\lambda_2\rangle = \frac{1}{4\pi}\sum_J (2J+1) d^J_{\lambda\lambda'}(\theta)\langle\lambda_1'\lambda_2'|V_\alpha^J|\lambda_1\lambda_2\rangle , \tag{4.11}$$

where $\lambda = \lambda_1 - \lambda_2$ and $\lambda' = \lambda_1' - \lambda_2'$, $d^J_{\lambda\lambda'}(\theta)$ are the reduced rotation matrices, and J is the total angular momentum of a given NN channel.

By inverting the above relation, one obtains

$$\langle\lambda_1'\lambda_2'|V_\alpha^J|\lambda_1\lambda_2\rangle = 2\pi \int_{-1}^{+1} d(cos\theta) d^J_{\lambda\lambda'}(\theta)\langle \mathbf{q}'\lambda_1'\lambda_2'|V_\alpha|\mathbf{q}\lambda_1\lambda_2\rangle \tag{4.12}$$

Finally, in the coupled $|LSJ\rangle$ representation, the matrix elements take the

form:

$$\langle L'SJ|V_\alpha^J(q',q)|LSJ\rangle = \sum_{\lambda_1\lambda_2\lambda_1'\lambda_2'} \langle\lambda_1'\lambda_2'|V_\alpha^J(q,q')|\lambda_1\lambda_2\rangle \times\langle L'SJ|JM\lambda_1'\lambda_2'\rangle\langle JM\lambda_1\lambda_2|LSJ\rangle \quad (4.13)$$

with

$$\langle LSJ|JM\lambda_1\lambda_2\rangle = (\frac{2L+1}{2J+1})^{1/2} C(LSJ;0\lambda)C(s_1s_2S;\lambda_1,-\lambda_2) \quad (4.14)$$

where $C(j_1j_2j;m_1m_2)$ are Clebsch-Gordan coefficients.

Note that a form factor of the type

$$\left(\frac{\Lambda_\alpha^2-m_\alpha^2}{\Lambda_\alpha^2+(q'-q)^2}\right)^{n_\alpha} \quad (4.15)$$

is applied to each meson-nucleon vertex, with the cutoff mass Λ_α and n_α as free parameters (see Table 4.1).

4.3 The $\rho N\Delta$ Contribution

Besides the exchange of heavy mesons between two nucleons, diagrams of the types shown in Fig. 4.2 can also occur. (We will limit ourselves to the case of a P_{33} isobar, given its dominant role).

The selection rules substantially reduce the number of bosons which can be exchanged in those diagrams: having the nucleon isospin $\frac{1}{2}$ and the Δ

isospin $\frac{3}{2}$, only an iso-vector boson ($T = 1$) can be present at the $\alpha N\Delta$ vertex, namely the pion and the ρ (besides the scalar δ, which we shall not consider).

To evaluate the contributions $V^{\alpha}_{N\Delta}$ and $V^{\alpha}_{\Delta\Delta}$, a procedure like the one described in the previous section is not directly applicable, as the OBE approach would allow for diagrams with more than three particles in the intermediate states, see Fig. 4.3, which are beyond the assumption of the model employed here. The procedure adopted is to simply include the ρ along with the pion in the three-body calculation. One writes the ρNN and the $\rho N\Delta$ vertices exactly as described in Section 3.1, and sums over the two possible values of the spin of the ρN pair ($\frac{1}{2}$ and $\frac{3}{2}$). The thus constructed potentials are then added to the corresponding pion-exchange terms, to give the full $N\Delta$ and $\Delta\Delta$ transition potentials

$$V_{N\Delta} = V^{\pi}_{N\Delta} + V^{\rho}_{N\Delta} \tag{4.16}$$

$$V_{\Delta\Delta} = V^{\pi}_{\Delta\Delta} + V^{\rho}_{\Delta\Delta} \tag{4.17}$$

For the $\rho N\Delta$ coupling constant, the quark model predicts [BW 75]

$$f^2_{\rho N\Delta} = \frac{f^2_{\pi N\Delta}}{f^2_{\pi NN}} g^2_{\rho NN} (\frac{m_\rho}{2M})^2 (1 + \frac{f_{\rho NN}}{g_{\rho NN}})^2 \tag{4.18}$$

with

$$f^2_{\pi N\Delta} = \frac{72}{25} f^2_{\pi NN} \tag{4.19}$$

and

$$f^2_{\pi NN} = (\frac{m_\pi}{2M})^2 g^2_{\pi NN} \tag{4.20}$$

($g_{\rho NN}$ and $\frac{f_{\rho NN}}{g_{\rho NN}}$ are given in Table 4.1.) At the $\rho N\Delta$ vertex, a cutoff as in Eq. (4.15) is applied, with $n_\alpha = 2$ (a dipole form factor is required to suppress the high momentum component at the vertex) and $\Lambda_\alpha = 1000$ MeV.

We point out that the present model does not contain any contribution of the type $\Delta\Delta\alpha$ (i. e. direct t-channel $\Delta\Delta$ OBE), contribution which is often neglected as no experimental information on the $\Delta\Delta$ coupling is available. This is a very reasonable approximation within a model for the NN interaction, where the effect of the direct term is usually minor [HM 87]; The same cannot be said for the elastic $N\Delta$ interaction [HM 87], which does play a role in pion-nucleus scattering and in the mechanism of Δ propagation in nuclear medium.

4.4 Preliminary Results

Here, we present and discuss phase shifts for some selected NN partial waves which indicate typical features as well as critical points of the model.

The curves shown here have been obtained without the inclusion of the deuteron channel. The reasons for this choice are technical (see Ch. 5 and Appendix), but a physical justification does exist: the effect of the πd channel on the NN inelasticities is essentially known [Lam+ 87] and rather small. We will, however, show in Ch. 5 its contribution to the pion production differential cross section, and we will discuss this point in somewhat more detail.

The present discussion can be subdivided into two major aspects: the short-range sector, which mostly effects the lowest partial waves, and the inelasticity problem, involving particularly those NN waves coupling to the dominant $N\Delta$ states (see Section 3.2).

In one of these aspects, or both, practically all models show some deficiencies; indeed, we can safely say that, up to date, only the low energy NN data can be accurately reproduced.

The short-range sector should be given priority when studying elastic

NN scattering, as the elastic NN observables are strongly sensitive to the description of the low partial waves. However, we stress again, this by no means implies an equally good description of the NN inelasticities or the πN system. We discussed this point in detail in Ch. 3 where it was shown how, for instance, the bad behaviour (strong attraction) of the $^3P_1$ phase shifts was at least in part related to the choice of a quantitative model for the P_{11}. Notice, however, that the use of the pole term only for the P_{11} does also give in general a poor $^3P_1$, (see Fig. 3.4).

We will discuss here another source of (intermediate-range) attraction, namely the two-pion exchange, Fig. 4.4. In the $OBEP$ approach, the fictitious σ is supposed to simulate this contribution, and, below the threshold, this model is known to work very well. Above the inelastic threshold, the $OBEP$ calculation is of course out of the question, as it would produce no inelasticity. Nevertheless, it is still interesting to notice that the real part of the phase shifts is, in some cases, better reproduced with $OBEP$ than with a model including the two-pion exchange.

In Fig. 4.5 we demonstrate this fact: the solid line is given by the standard model as described in Ch. 3 (the pole and the non-pole parts are used for the P_{11}, with off-shell cutoff of 1.2 GeV for both, and a cutoff of

0.8 GeV for the P_{33}); the dashed curve is obtained by simply suppressing the P_{33} channel in the standard calculation. Both of these curves do not include short range contributions, as the present purpose is to isolate the effect of the attraction from the 'Δ-box' diagram, Fig. 4.4. Finally, the dotted curve is a true $OBEP$ from Machleidt [Mac 88].

Obviously, we must be looking at some overestimation of the intermediate-range attraction. Against our expectations, this problem has not been cured by the $\rho N\Delta$ contribution, which is included in the curves shown in Fig. 4.6-8.

The parametrization adopted (Table 4.1) was chosen so to achieve a good fit of $^1D_2$; actually, a satisfactory fit of this wave was first obtained with the inclusion of heavy-meson exchange in the NN channel only, and then, after including the $\rho N\Delta$ contribution, the parameters were readjusted so to regain the previous fit of $^1D_2$. In conventional low-energy NN models [MHE 87], a large effect is observed by applying this 'refit' procedure to the S waves at low energy. Presumably, a more careful study of the ρ parametrization is needed: for instance, choosing to fit $^1D_2$ to begin with may already prejudice the analysis against lower partial waves. In other words, the net effect of a heavy meson (since it is introduced, up to a

certain extent, phenomenologically) does depend on one's reference point in defining the effect itself.

Besides the criteria for choosing the one-boson-exchange parametrization, more substantial differences exist between the NN two-body models and the πNN theories (such as ours), which may strongly effect the quality of the predicted NN phase parameters. In the πNN models, as explained in Section 2.2, the two-baryon intermediate state is represented by a spectator nucleon and an interacting πN pair (the isobar). These considerations lead to the expression Eq. (2.9) for the nucleon propagator. In conventional two-body model, (where usually the BbS equation is applied to the two-nucleon system), the BbS choice [BS 66] for the covariant propagator (reduced to a three-dimensional form by assuming that the two nucleons are equally off-shell) is the most widely used. For an extensive discussion on this and other choices suggested in the literature, see Machleidt [Mac 88]. Here, we just mention that the different energy dependences of the two-nucleon propagator in the two approaches (NN and πNN) does have consequences (including different convergence properties of the equation). The particular structure of the NN propagator in the πNN framework does in fact contribute (among other features already discussed) to the typical

tendency of the predicted NN P-waves. (We recall that, for the P-waves, the NN intermediate states are at least as important as the $N\Delta$ states; see p. 41.)

As far as $^1D_2$ and $^3F_3$ are concerned, the major problem is in the inelasticity, as already discussed in Ch. 3 in relation to off-shell effects. For $^1D_2$, a rapid decrease of the inelasticity is observed above 600 MeV, in disagreement with the analysis of Arndt et al. [Arn+ 83] but consistent with the Saclay data [Bys+ 84]. Interestingly, in other models [Lom 82, Mac 88] a similar decrease, or at least saturation of the inelasticity, is predicted.

Some comments may be appropriate here concerning the model of Pöpping et al. [PSZ 87] which, unlike most of the others, does surprisingly well with the NN phase parameters (real phase shifts and inelasticities). This is a force model based on a hamiltonian approach in the framework of non-relativistic quantum mechanics. From the discussion in Section 3.2, one may conclude that a more sophisticated model for the Δ resonance is indispensable for an improved description of the NN inelasticities. It is therefore not clear to us how a relatively simple approach such as in the model of Pöpping et al. [PSZ 87] can achieve what is probably the best fit of the NN phase parameters over all the intermediate energy range. In particular,

we notice that their model for the Δ isobar is far from being sophisticated; moreover, a very strong cutoff (about 300 Mev) is used for the $\pi N\Delta$ vertex, which would usually produce rather small inelasticities, specifically in the triplet ${}^3F_3$ (hence, the necessity for off-shell modifications; see Section 3.2).

Finally, the phase shifts for some of the peripheral waves are shown in Fig. 4.8. As mentioned above, it has often been pointed out in the literature that pion production appears to be a rather peripheral mechanism; we are now in the position of verifying the above statement, which will be done in the next chapter.

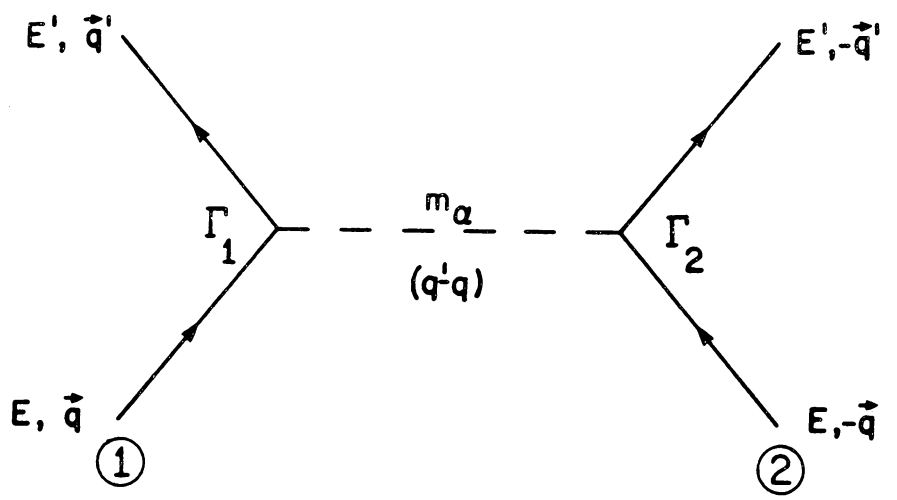

Figure 4.1: **Feynman diagram representing a one-boson-exchange contribution to NN scattering in the C. M. frame.** Full lines denote nucleons, the dashed line a boson with mass m_α.

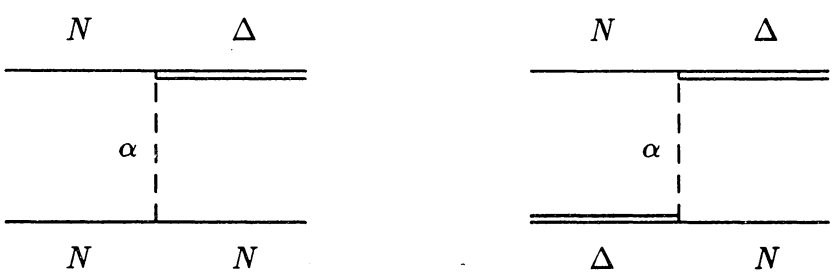

Figure 4.2: One-boson-exchange diagrams involving a Δ-isobar;

(a) $V^{\alpha}_{N\Delta}$, (b) $V^{\alpha}_{\Delta\Delta}$.

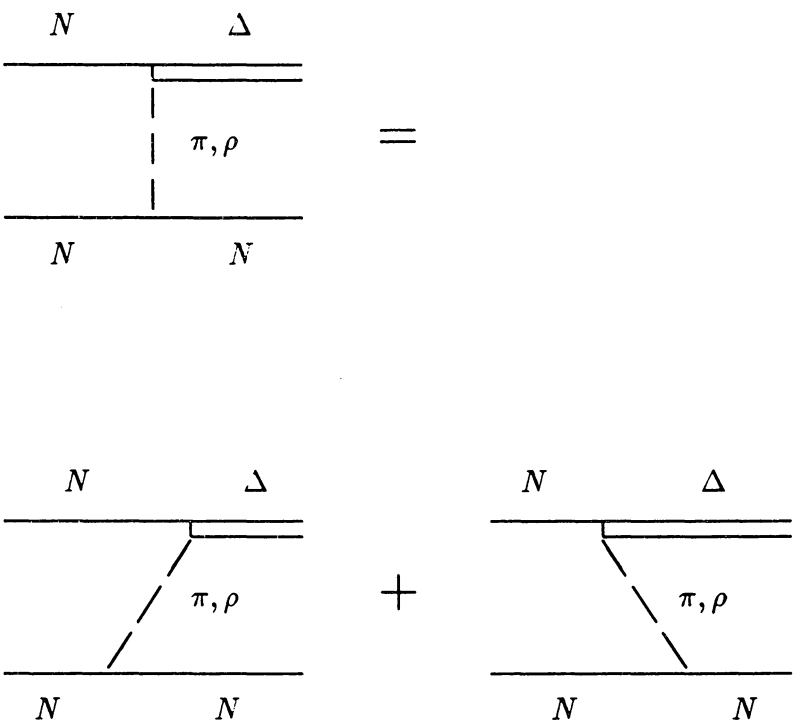

Figure 4.3: Time-ordered one-boson-exchange diagrams.

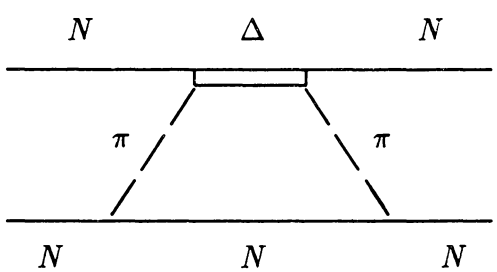

Figure 4.4: 2π-exchange diagram.

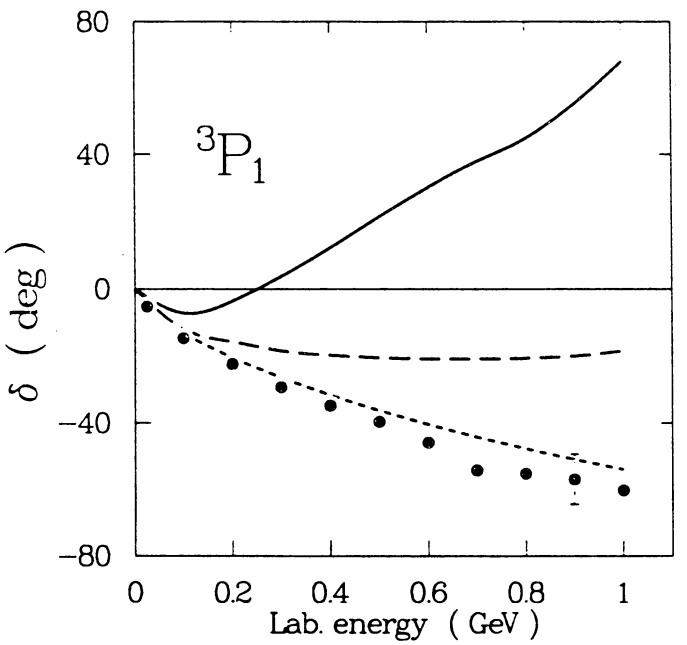

Figure 4.5: $^3P_1$ **phase shift as from our standard model (solid), suppressing the P_{33} channel (dashed), and from the OBEP of [Mac 88] (dotted).** Data from Arndt et al. [Arn+ 83].

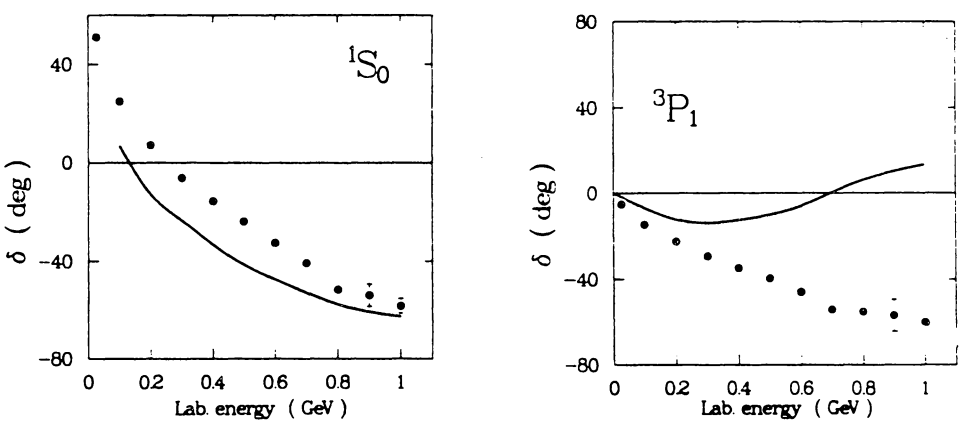

Figure 4.6: $^1S_0$ and $^3P_1$ phase shifts as predicted by our model. Data from Arndt et al. [Arn+ 83].

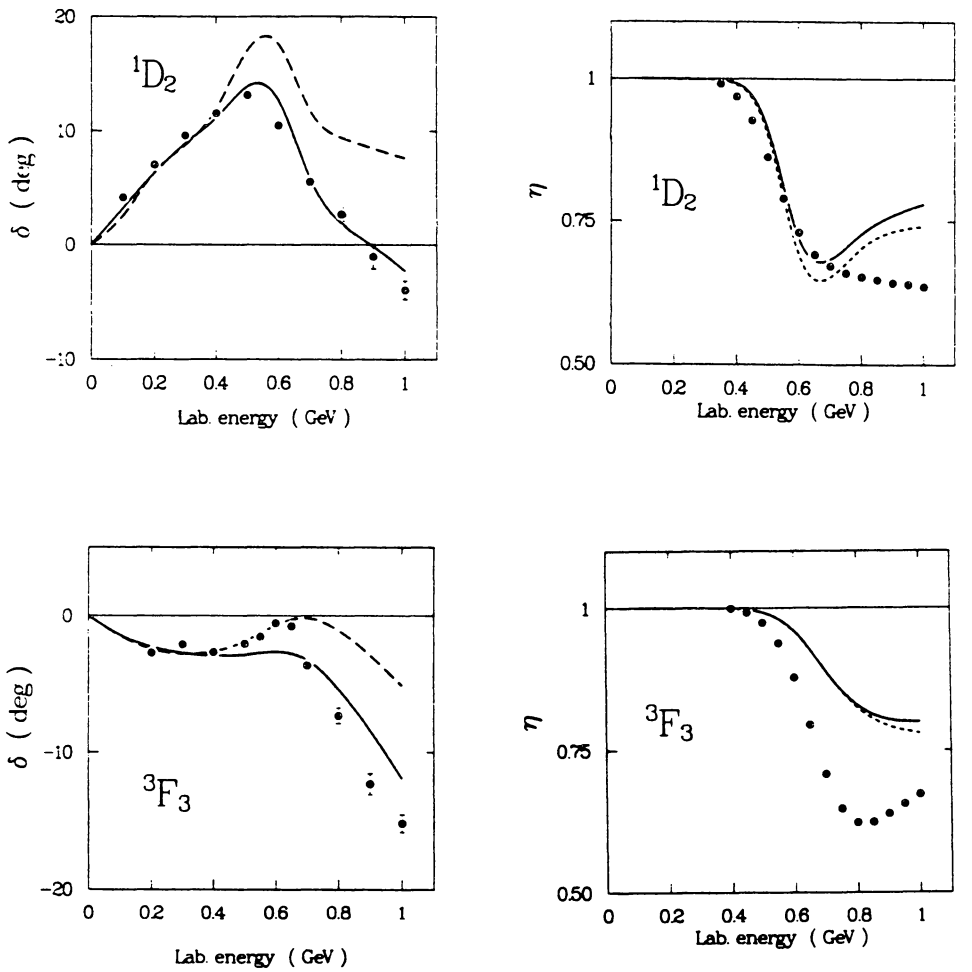

Figure 4.7: **Phase shifts and inelasticity parameters for $^1D_2$ and $^3F_3$.** Solid line with and dashed without short range contributions. Data from Arndt et al. [Arn+ 83].

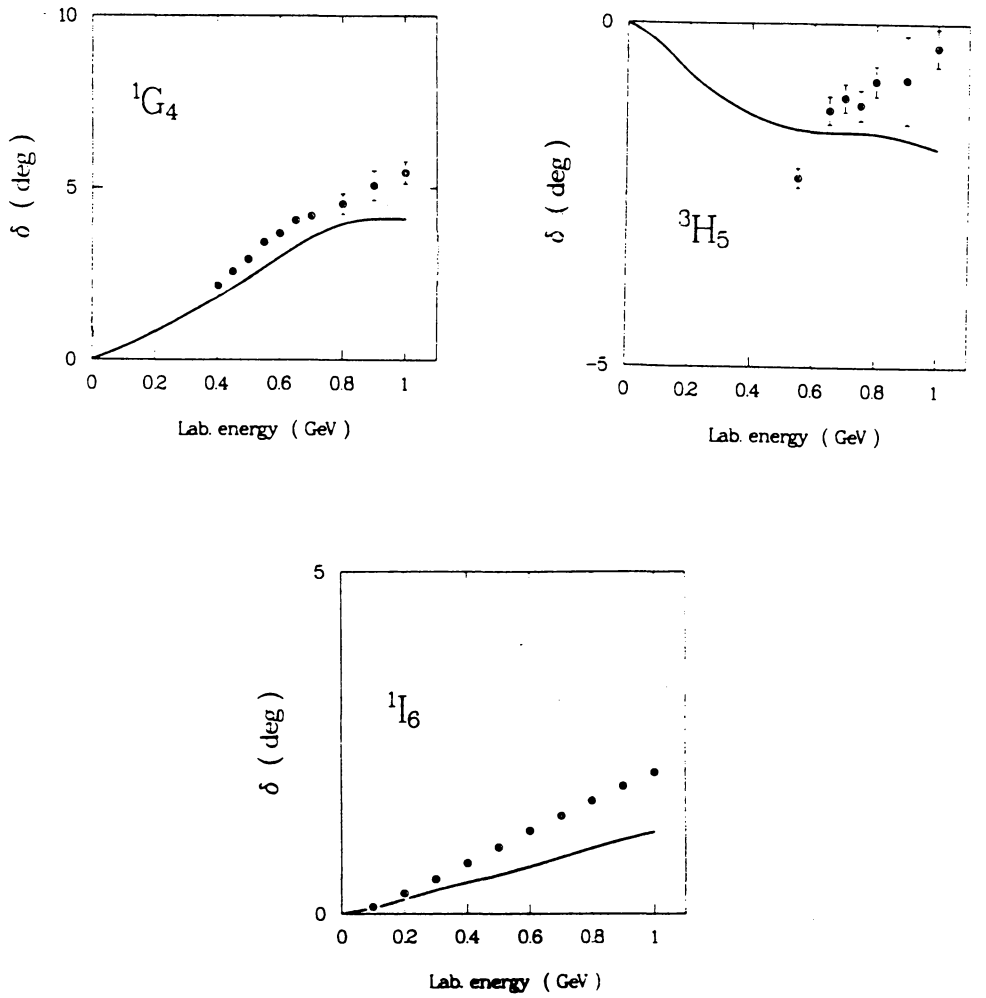

Figure 4.8: **Phase shifts for some peripheral waves as predicted by our model.** Data from Arndt et al. [Arn+ 83].

Table 4.1: **Meson parameters used for one-boson-exchange.**

	m_α (MeV)	$g^2/4\pi$	Λ_α (MeV)	n_α
σ	570	7	1300	1
ω	782.8	22	1650	3/2
ρ	769	0.7 (6.1)[a]	1400	3/2

[a] The tensor/vector ratio of the ρ coupling constants, f/g, is given in parenthesis. For the ω this ratio is assumed to be zero.

Chapter 5

The Pion Production Channel

5.1 Introduction

The $NN \rightarrow \pi NN$ reaction has been studied rather intensively in the past five years, but still not exhaustively. Because of its much richer final phase space, the $2 \rightarrow 3$ body unbound process is technically more difficult to handle, theoretically and experimentally. Predictions for $NN \rightarrow \pi NN$ spin observables are available [DKS 87, ML 86, Dub+ 86] and recently other authors [Ued 86b] have begun to look at this process; on the experimental side, data on the spin dependence of this reaction are scarce [Han+ 83, Wic+ 86] and often beset with large uncertainties. A growing interest

is, however, developing around this process (for instance, the database is rapidly expanding), as its knowledge is indispensable for a detailed understanding of NN inelasticities.

In the following sections, we describe how the production mechanism is incorporated in our model; we then present some predictions for spin observables, comparing with data wherever available. We will concentrate, in this work, on exclusive processes (kinematically complete experiments). This case is simpler from the technical point of view since no integration in the final phase space is necessary; also, some data do exist, as well as calculations. Even when data are not available, we shall try to compare with the predictions from other models: this is a useful consistency check, and also serves to elucidate the model dependence of the predictions.

5.2 The $2 \rightarrow 3$ Body Amplitude

For the reaction we are studying, the initial channel is always a two-nucleon state on-shell; therefore, we solve the integral equation, Eq. (2.4), for half-off-shell isobar amplitudes describing the process $NN \rightarrow N\alpha$ (α is the isobar label); see Appendix A for details on the numerical integration. The

subsequent isobar dissociation is then calculated from those amplitudes, as schematically described in Fig. 5.1. In the figure, $\mathbf{p}_1$ and $\mathbf{p}_3$ are the momenta of the final nucleons, and $\mathbf{p}_2$ is the pion momentum.

To explain more concretely the technical aspects (concerning the construction of the $2 \rightarrow 3$ body amplitude), we will specifically consider the case of a proton and a π^+ emitted from a double-charged P_{33} isobar (Δ^{++}), with the neutron (usually undetected) as the spectator (as we shall see, this is the dominant mode for π^+ production).

Treated consistently with what was explained in Ch. 3 [see Eq. (3.2)], the isobar dissociation vertex has the form

$$\begin{aligned}\langle \mathbf{p}_1, m_1' | \alpha, -\mathbf{p}_3, m_\alpha' \rangle &= \sum_\lambda \langle 1, \frac{1}{2}, \lambda, m_1' | \frac{3}{2}, m_\alpha' \rangle \frac{V(Q)}{Q} \times \\ &\times \{ p_1 Y_1^\lambda(\hat{\mathbf{p}}_1) + \rho(p_1, p_3, z) p_3 Y_1^\lambda(\hat{\mathbf{p}}_3) \} \ , \quad (5.1)\end{aligned}$$

where V is the form factor, and

$$\mathbf{Q} = \mathbf{p}_1 + \rho(p_1, p_3, z)\mathbf{p}_3 \qquad (5.2)$$

[see Eq. (2.14)]. Eq. (5.1) is nothing but Eq. (3.2) where explicit values of the spins and the orbital angular momentum l have been inserted for the

case $\Delta \rightarrow N\pi$. Also, we have used

$$Y_1^{\lambda}(\hat{\mathbf{Q}}) = \sqrt{\frac{3}{4\pi}}\frac{1}{Q}Q_{\lambda} \tag{5.3}$$

where Q_{λ} is the spherical component of the vector $\mathbf{Q}$.

The (LSJ) projections of the isobar amplitudes are then summed over to provide the (two-body) plane-wave amplitude. Choosing the quantization axis along the incident direction, which we take to be the z-axis, we obtain

$$\begin{aligned}\langle m'_{\alpha}, m'_2, \mathbf{p}_3|T|m_1, m_2, \mathbf{p}\rangle \;=\; & \sum_{L,S,L',S',J} \langle \frac{1}{2}, \frac{1}{2}, m_1, m_2|S, \gamma\rangle\langle L, S, 0, \gamma|J, \gamma\rangle \\ & \times \langle \frac{1}{2}, s_{\alpha}, m'_2, m'_{\alpha}|S', \gamma'\rangle\langle L', S', \mu', \gamma'|J, \gamma\rangle \\ & \times Y_{L'}^{\mu'}(\hat{\mathbf{p}}_3)\sqrt{\frac{2L+1}{4\pi}}\end{aligned} \tag{5.4}$$

Finally, after summation over the isobar spin projections, the product of the plane-wave amplitude, the isobar propagator and the break-up vertex provides the $2 \rightarrow 3$ body spin amplitude

$$T_{23} = \langle m'_1, m'_2, \mathbf{p}_1, \mathbf{p}_2|T|\mathbf{p}, m_1, m_2\rangle = \sum_{m_{\alpha}} \langle \mathbf{p}_1, m'_1|\alpha, -\mathbf{p}_3, m'_{\alpha}\rangle R(\sigma_{p_3}) T_{N\alpha} \tag{5.5}$$

with $T_{N\alpha}$ as in Eq. (5.4), and σ the invariant mass of the isobar (which depends only on p_3; see Fig. 5.1).

Notice that we compute the $2 \rightarrow 3$ body amplitude in the overall C.M.;

actually, the kinematical variables assigned by the experimental conditions are boosted to provide the corresponding C.M. quantities, which we use in the calculation of T_{23}. Since the vector **Q** at the vertices (see Ch. 2) allows the angular momentum to be treated in a covariant way [AAY 68], Eq. (5.5) is an invariant quantity [DKS 87] and can be used to evaluate observables in the laboratory system.

A boost of the final nucleon spin states (Wigner rotation) does, usually, give a very small correction [DKS 87]; for those observables which involve either initial spin or final spin determination, this complication does not need to be taken into account: as the direction of the boost is along the quantization axis, the spin projection (for the initial state only) identifies with the helicity, which is conserved under a Lorentz transformation along the z-direction. Only the observables involving determination of one initial and one final spin along the boost direction are affected by the relativistic spin precession, for instance the spin-transfer coefficient D_{LL} (at the energies under consideration, however, the Wigner rotation angle is usually a few degrees [Sil 88]).

The full (ninefold) differential cross section equals, up to phase space

and flux factors, the square of T_{23}:

$$d\sigma = \frac{(2\pi)^4 |T_{23}|^2}{4F} \delta^4(P - \sum_{i=1}^{3} p_i) \prod_{i=1}^{3} \frac{d^3 p_i}{(2\pi)^3 2E_i} \tag{5.6}$$

where F is the invariant flux (in the laboratory system, $F = p_{lab} m$). Actually, only five variables are needed to fully specify the final state, given the energy-momentum conservation relations expressed by the $\delta-$ function.

As is usually done in the case of two charged particles, we choose to specify the proton and pion directions and the proton final momentum; the remaining variables will be formally integrated over, giving the fivefold differential cross section.

Asymmetries and spin-spin correlations can be expressed in terms of differences of polarized cross sections; see Appendix B for more details.

5.3 Results

We will present predictions obtained with the basic πN input as described in Ch. 3; variations in the input will be specified as they occur. The πd channel is not included, except for the subsection where we explicitly discuss this contribution.

We allow for π^+ production through Δ^{++} and Δ^+ isobars (as we will

show, this is a very good approximation; indeed, the contribution from Δ^{++} alone gives practically all the cross-section). In what follows, the two specified angles (θ_p, θ_π) refer to the outgoing proton and pion, respectively, in the laboratory system, and are located in the scattering plane. Out-of-plane measurements are also possible, but there is very little such measurement so far.

First, we show the calculated energy dependence of the differential cross section for fixed kinematical configuration (Fig. 5.2). Notice the different horizontal scales, due to a different domain of physical solutions for the kinematical equations. One may observe that the increase of the predicted cross section after 570 MeV is not very rapid; not surprisingly, the insufficiency of the predicted inelasticities in the major singlet and triplet reflects itself in the cross section.

This is fully confirmed by Fig. 5.3, where the cross section (the low-momentum region is discussed later in this chapter) is compared with the data [Han+ 83] for two different kinematical situations, and where the solid curve is obtained with our standard model as described in Ch. 3, with off-shell modifications for the P_{11} and the P_{33} (cutoff of 1.2 GeV for the pole and non-pole parts of the P_{11} and 0.8 GeV for the P_{33}).

A check of consistency can be performed by looking at the same quantities in other models [ML 86, DKS 87] in relation to the predicted inelasticities. The model of [DKS 87] substantially overpredicts $^1D_2$ (at 800 MeV, about 70 degrees for the inelasticity parameter, against 25 from the phase shift analysis); the triplet $^3F_3$ is also above the experimental value, but not as much (and it is slightly underestimated above 1 GeV). Their differential cross section is however not drastically overestimated; for certain forward kinematical configurations, as the one considered in Fig. 5.3, it is actually only slightly overpredicted [DKS 87]. This raises the question on the relative importance of the singlet and the triplet at this energy, or, in other words, if and where the triplet starts to dominate the cross section. We will come back to this point later in this section, performing an analysis in partial waves of these observables, to isolate various contributions.

To better establish the correspondence between the major inelasticities and the size of the predicted cross section, we have performed some variations of the model. For the dashed curve shown in Fig. 5.3, we have used a rank-one P_{11} (pole part only) with an energy-independent monopole form factor, as in the Kloet-Silbar work [KS 80]. We have kept our model for the P_{33} as well as the off-shell modifications but have 'artificially' increased

the inelasticity with a cutoff of 1.2 GeV for the P_{33} (a value of 0.8 GeV is used for the solid curve). We recall how this choice creates attractive side effects; see Fig. 3.2. The inelasticities in $^1D_2$ and $^3F_3$ corresponding to the dashed curve in Fig. 5.3, in terms of η, are 0.40 and 0.73 respectively (the values from the phase shift analysis [Arn+ 83] are 0.65 and 0.62).

The dash-dotted curve in Fig. 5.3 is obtained as above, but with an off-shell cutoff of 1.5 GeV for the P_{11}. (As expected from the discussion in Ch. 3, in particular Fig. 3.4, such a large cutoff mass, used in a rank-one P_{11} potential, considerably reduces the attraction in the NN P-waves.)

Notice from Fig. 5.3 that the overestimation of the inelasticity in $^1D_2$ does not imply a similar overestimation of the cross section. We must also mention that, in achieving larger inelasticities, a strong attraction has been produced: $\delta(^1D_2)$ is about 20 degrees at 800 MeV. This is a behavior rather similar to that found by Kloet and Silbar [KS 80].

What we have learnt from the above is the following: it is indeed possible to increase the inelasticity, and, correspondingly, the cross section, as expected, but some kind of price must be paid. In particular, if this is achieved by varying off-shell parameters, it appears that an overly strong attraction cannot be avoided. Also, the description of the P_{11} seems to

strongly affect the inelasticity in ${}^1D_2$ (in favor of a rank-one potential, namely a less realistic description of the P_{11}). On the other hand, the cross section does not seem to be much disturbed by any of these side effects, and it can be actually fitted by simply controlling the inelasticity.

Recently, a different analysis [Wic+ 86] of the $pp \to pn\pi^+$ process has provided cross section and polarization information for the process $pp \to n\Delta^{++}$, by selecting from the raw data the events with a $p\pi^+$ correlated pair. We have studied this process as a further consistency check of our three-body final state calculation, since we are obviously looking at different analyses of the same problem. The results are shown in Fig. 5.4, where the same study as that in Fig. 5.3 is performed. As to be expected, the solid curve underestimates the cross section by about the same amount as in Fig. 5.3 (there where both cross sections are the largest), and very similar effects are obtained with the modifications explained above.

Next, we show how the clear underprediction of the solid curve in Fig. 5.3 is seen in other exclusive differential cross sections (Fig. 5.5). As less production occurs, the model does better at reproducing the experimental production, as seems reasonable: the cross section is basically 'background', in the sense that the isobar is not at the resonance. For these cases, the

disagreement (solid curve in Fig. 5.5) becomes less drastic, and the modified models tend to overpredict the cross section.

We recall that, in an experiment with exclusive kinematical conditions, energy-momentum conservation dictates the kinematics of the undetected variables, and therefore the value of the isobar invariant mass. This in turn controls the break-up probability, i.e. the cross section (up to a two-fold ambiguity, in those cases where two physical solutions for the undetected momentum exist.)

In what follows, we will use our standard model (solid curve in all figures of this chapter), as it is our intention to learn more about it through the study of the production channel, rather than fitting observables by the introduction of 'ad hoc' modifications.

Up to now, we have concentrated on understanding what builds up the cross section. Next, we will further analyse the features of the model through the study of spin observables. Because these depend more on relative phases of amplitudes, we expect them to be more sensitive to different, and more subtle, aspects of the theoretical input.

The beam asymmetry, A_{N0}, is essentially the only other exclusive observable for which a reasonable set of data [Han+ 83] is presently available.

From Fig. 5.6-8, we observe a reasonable agreement with the low- momentum part of the data; the model, however, totally fails to follow the rise of the data in the high momentum part, where the theoretical curve shows no structure at all. The rise of the polarization data at high momentum may not be explained by a simple argument [Sil 88], and therefore this could be a key area for future attempts at understanding the model dependence of this process.

If the behaviour of the cross section can be easily understood, the same cannot be said for the polarization, which, as already mentioned, depends sensitively on relative phases between different amplitudes. It is therefore of crucial importance that the phase information of each amplitude is treated correctly, as even smaller amplitudes may interfere to give a significant contribution.

To better understand the structure of the polarization, and following Dubach et al. [DKS 87], we have compared A_{N0} with A_{0N}, the target asymmetry (Fig. 5.9): clearly, $A_{N0} \approx -A_{0N}$; in fact, it can be shown [DKS 87] that, if these two spin observables are only due to the interference of two partial waves of opposite parity, the equality is exact. The approximate equality of our predicted A_{N0} and $-A_{0N}$ suggests that we are looking at

quantities controlled by the interference of two amplitudes both of which lack strength; naturally, one immediately thinks of the major singlet and triplet waves, ${}^1D_2 \rightarrow {}^5S_2$ and ${}^3F_3 \rightarrow {}^5P_3$. A similar correlation between the lack of inelasticity in the triplet channel and the quality of the predicted longitudinal asymmetry, $\Delta\sigma_L$, can be observed [KS 81, DKS 87].

In Fig. 5.10-11, we also show our predictions for some spin-spin correlations (both beam and target polarized) at two different kinematical conditions. Some qualitative similarity can be observed with the corresponding predictions from Dubach et al. [DKS 87], for instance in the large and negative A_{NN}, and in the way some spin-spin correlations relate to each other. For example, notice that A_{LL} and A_{SS} are roughly the same. In general, no strong energy dependent structures are observed.

Now, we want to analyse some of these spin observables in terms of various contributions to better understand what controls them.

Contributions of low partial waves:

The effect of contributions of low partial waves is shown in Fig. 5.12. As already pointed out by Dubach et al. [DKS 87], the central partial waves seem to interfere with higher J amplitudes so as to reduce the cross section. This is clearly confirmed in the figure, where the dashed curve does

not include the $J = 0, 1$ partial waves. A rather small effect is observed on A_{N0}. It appears, however, that the spin-spin correlations are somewhat more sensitive to those contributions; an example is shown in Fig. 5.13, where we have chosen a kinematical configuration for which a similar study has been performed [DKS 82]; we find a clear similarity with the prediction of A_{LL} from that work, and the consequences of omitting the central waves. The dotted curve is also from Dubach et al. [DKS 82].

Relative importance of $^1D_2$ *and* $^3F_3$*:*

The effect on the differential cross section from omitting the major triplet wave is strikingly larger than the one obtained from omitting $^1D_2$ (Figs. 5.14-15). Notice that the predicted inelasticity for the latter is numerically larger, at 800 MeV (see Ch. 4). Nevertheless, it appears that, at this energy, production from a $N\Delta$ channel in a relative P-wave, for typical exclusive kinematics, is the preferred mechanism. Even in the work of Dubach et al. [DKS 87], in spite of the substantially larger $^1D_2$ inelasticity, the differential cross section is more reduced by omitting the triplet. The beam asymmetry is about equally sensitive to both contributions and much smaller in magnitude, as expected from the above considerations of interference.

Spin-state effects:

When the major singlet is shut off, or when all the NN singlets are omitted (compare Fig. 5.14 and 5.16), the effect on the cross section is very similar. Notice, however, the polarization in the absence of the singlets (Fig. 5.16) and compare with Fig. 5.9: in the region where A_{N0} and $-A_{0N}$ are practically identical no asymmetry is observed when the waves of positive parity are omitted. Elsewhere (e. g., at low momentum), some asymmetry must be produced by the triplets alone. When all the triplets are shut off, the asymmetry is obviously zero, as no LS force is generated. The cross section (Fig. 5.17) is comparable to the one obtained by omitting the major triplet only. It appears that a pure spin-state analysis confirms the conclusions already made regarding the two dominant partial waves, for both the differential cross section and the polarization. As far as the spin-spin correlations are concerned, notice the large values of A_{LL} (Fig. 5.18) in the absence of either one of the major waves. One could argue that these are due to the interference with the background partial waves. However, since the longitudinal spin states are simply $|+\frac{1}{2}\rangle$ and $|-\frac{1}{2}\rangle$, the expression

for A_{LL},

$$A_{LL} = \frac{\sigma(L,L) - \sigma(L,-L)}{\sigma(L,L) + \sigma(L,-L)} \tag{5.7}$$

reduces essentially to the difference of two cross sections with initial spins parallel and antiparallel respectively. The fact that in the absence of $^3F_3$ ($^1D_2$) A_{LL} is close to -1 ($+1$) is then a further indication that $\sigma(L,L) \approx \sigma(^3F_3)$ and $\sigma(L,-L) \approx \sigma(^1D_2)$.

Short-range effects:

Short-range effects are, of course, expected to affect mostly the central waves, and their contributions have already been shown in Figs. 5.12-13 to be rather small in the cross section and asymmetry and more noticeable in the spin-spin correlations. The cross section (Fig. 5.19) is slightly reduced, consistent with the fact that the inelasticities are reduced by the inclusion of short range forces. A little more structure seems to be achieved in the asymmetry, but no drastic change is observed.

Recent results of our group [MF 88] on the process $pp \to n\Delta^{++}$ seem to indicate some sensitivity of A_{N0} to short-range effects. It appears, actually, that this quantity is better described without the inclusion of heavy meson exchanges. However, these results have been obtained within an improved model for the P_{33} (see Ch. 6) which has not yet been applied to

the production channel.

Other effects:

We have also investigated other aspects of the model. We show in Fig. 5.20 how the small πN waves have minimal effect on this process.

In Fig. 5.21 we have isolated the contribution from production through a Δ^+ isobar decay, $\Delta^+ \rightarrow n\pi$, in the presence of a spectator proton.

We finally show (Fig. 5.22) how a first order approximation (Born or impulse approximation) predicts the cross section. The corresponding predicted asymmetry, however, is practically zero. We recall that the Born approximation is rather reasonable for the higher partial waves; these contributions are mainly real, i.e. their relative phase differences should be small; the fact that this approximation produces a significant amount of cross section is consistent with the statement that pion production is a peripheral process.

The deuteron channel:

The πd channel has so far been neglected, and the reason is essentially technical: as explained in the appendix, the inclusion of this contribution substantially increases the numerical difficulties of the calculation and, most of all, the computing time. However, when looking at the pion production

mechanism to learn about the off-shell πN physics, as done in this work, it is reasonable to believe that the deuteron channel is not of crucial importance (after all, its effect on the inelasticities, especially at 800 MeV, is rather mild [Lam+ 87]). We stress that this statement refers to the relative importance of the deuteron as compared in particular to the P_{33} for the understanding of the NN inelasticities. This channel becomes, however, essential when one wants to explain all the features of the cross section: the smaller rise of the data at low momentum (see, for instance, Fig. 5.3) is due to the NN final state interaction (FSI), i. e. scattering of the two final nucleons when emitted at relatively low momentum. Obviously, we are now dealing with a different type of physics. On the other side, the largest part of the cross section, as should be clear by now, can be explained as long as enough inelasticity is predicted.

Here we only report our result for the differential cross section with the inclusion of the $^3S_1$ NN channel (as described in Ch. 3) in the intermediate states only (Fig. 5.23). No further NN interaction is taken into account at the three-body final state level. Not surprisingly, the peak region, where the Δ dominates, is practically uneffected; at low momentum (where the isobar is obviously off the resonance), the effect is small but noticeable. The fact

that only a very small enhancement at low momentum is observed is actually rather interesting: first of all, one may conclude that the interaction of the two nucleons in the intermediate states is obviously not sufficient to describe the FSI (this may seem an obvious remark, but questions of double counting may in principle not be completely clear); secondly, the question of the importance of the singlet $^1S_0$ occurs. Even though the $^1S_0$ final NN state is suppressed in $NN \to \pi NN$ reactions because of selection rules, it has been found [DKS 86] that both states can interfere dramatically. In the work of Dubach et al. [DKS 86] FSI corrections are taken into account by multiplying the T-matrix by a factor which incorporates the FSI between the final nucleons in relative S-waves. It would certainly be interesting to see whether or not the inclusion of the singlet state produces substantial enhancement even in absence of FSI, i. e. by inclusion of another 'direct' two-body NN interaction. At this stage, given the complexity of the calculation when the deuteron channel is included, we will postpone the investigation of this problem, which however remains among our plans for the nearest future.

In the above, we have tried to analyse critically the major ingredients of the model; some typical features, as well as deficiencies, show up clearly.

Before attempting predictions for more complicated processes, which would necessarily bear a trace of these deficiencies, we believe we can draw from the present work some definite conclusions, which are suggestive of a possible way to proceed.

Those conclusions, as well as our future plans, are summarized in the next chapter.

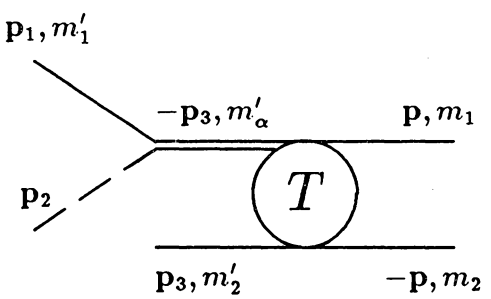

Figure 5.1: **Schematic representation of the $2 \to 3$ body amplitude.**

The underlying time axis is horizontal, pointing left into the future.

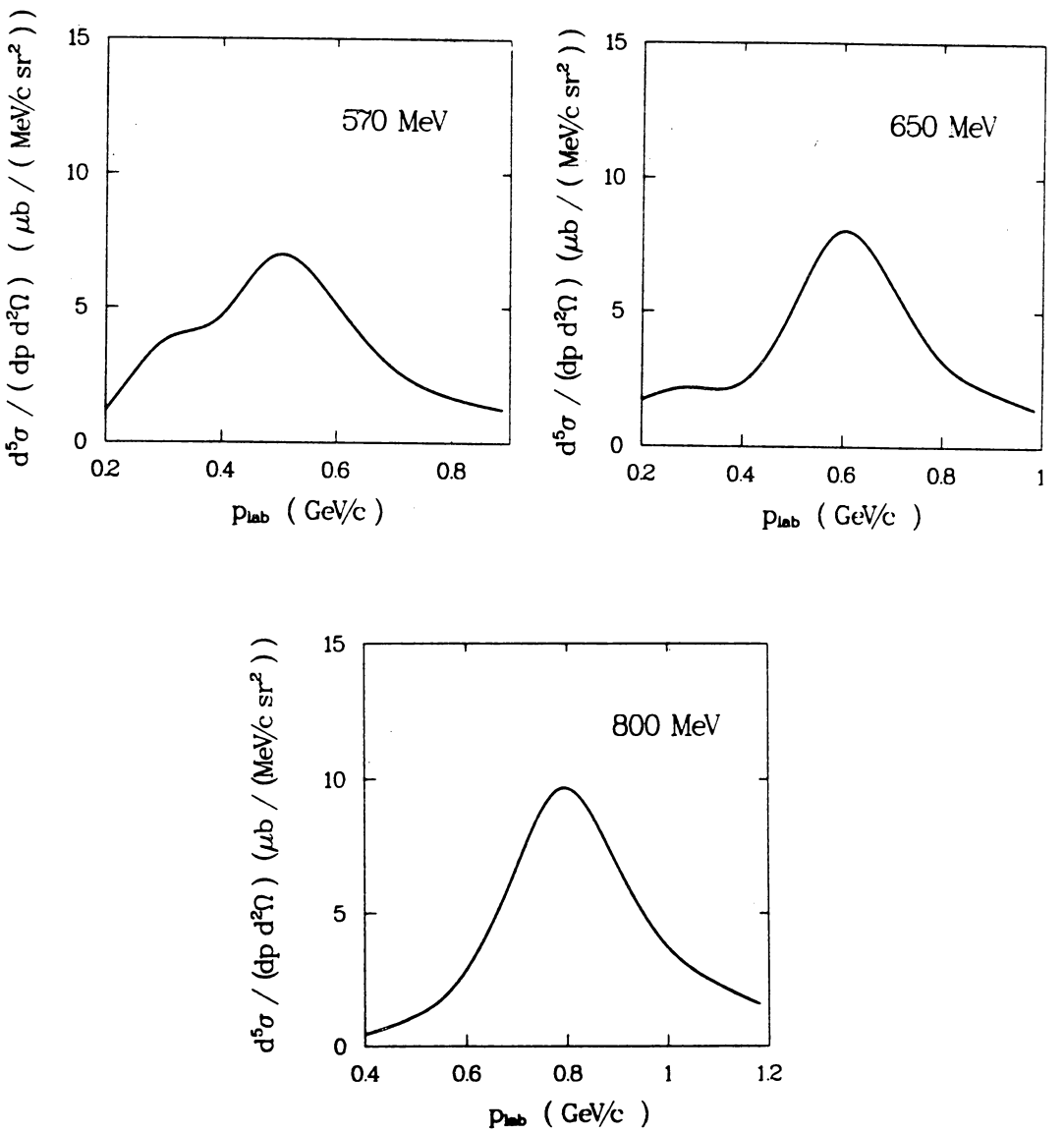

Figure 5.2: Energy dependence of the differential cross section at (14.5°, 21°).

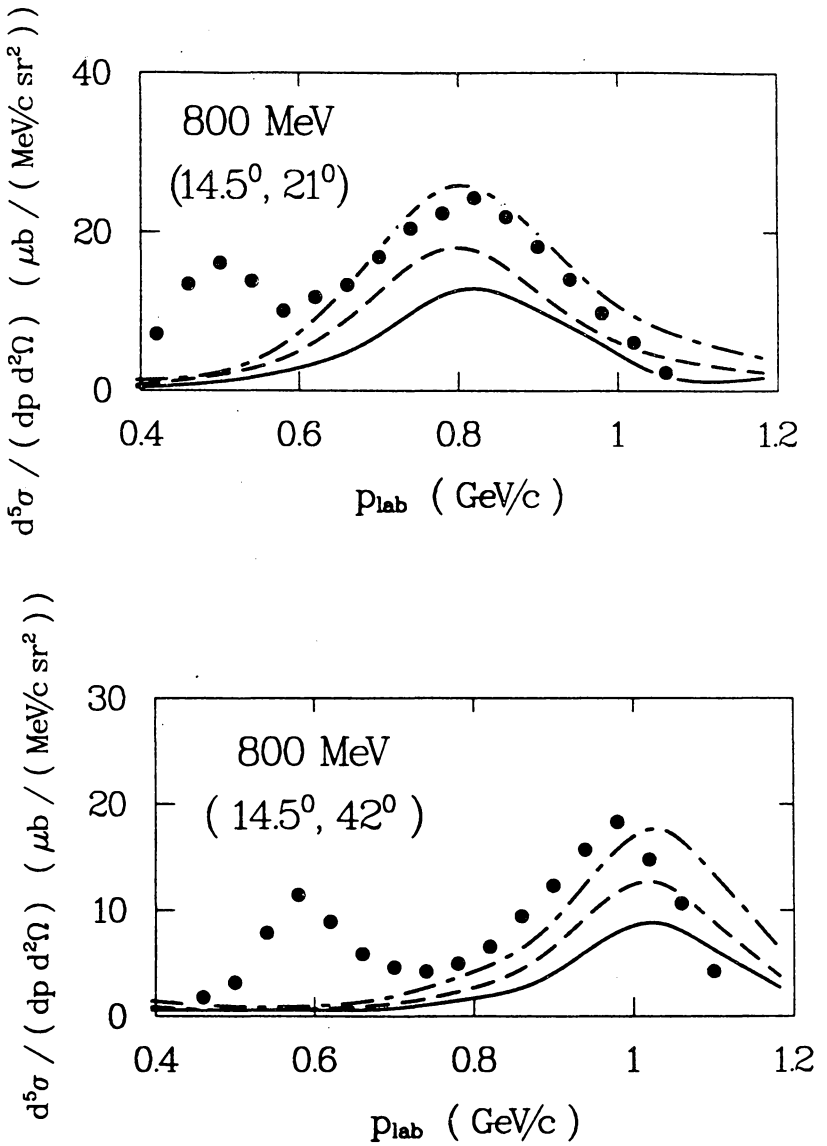

Figure 5.3: **Predicted $pp \to pn\pi^+$ cross section obtained with our model (solid) and variations thereof (dashed and dash-dot) as explained in the text.** Data from Hancock et al. [Han+ 83].

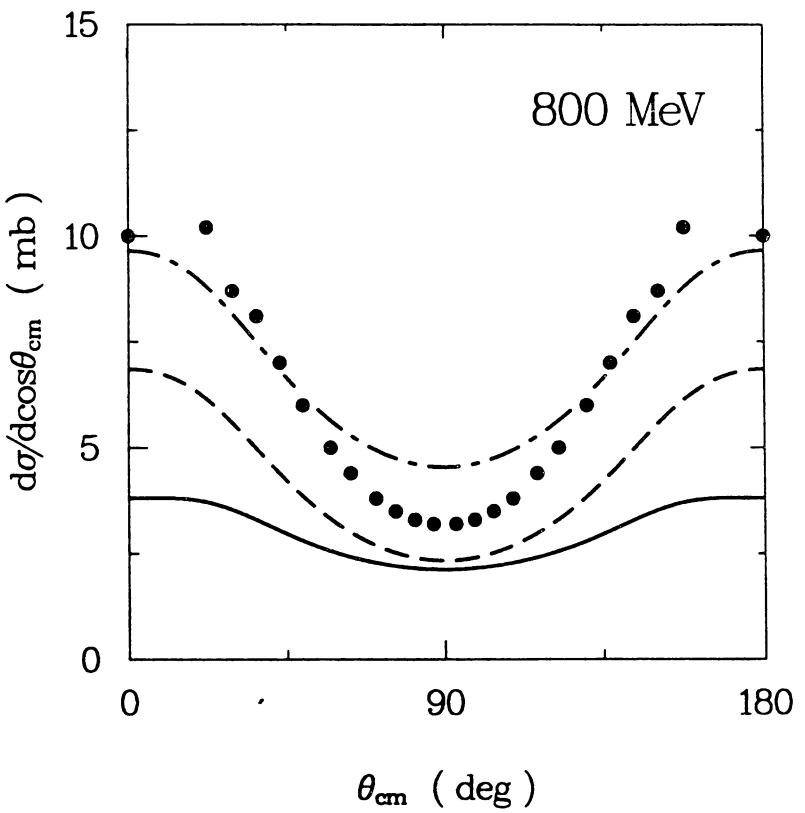

Figure 5.4: **Same as Fig. 5.3 for the process $pp \rightarrow n\Delta^{++}$.** The Δ-invariant energy is 1.238 GeV. Data from Wicklund et al. [Wic+ 86].

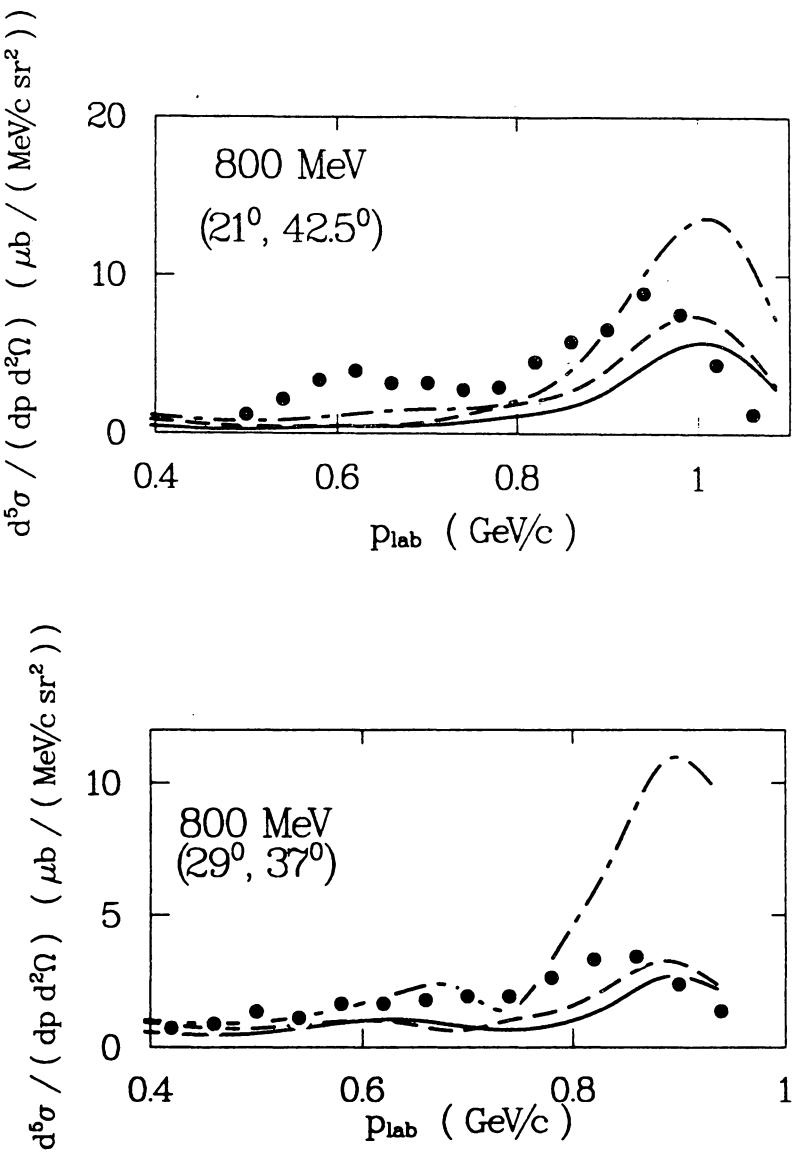

Figure 5.5: Same as Fig. 5.3 for different kinematical conditions.

Data from Hancock et al. [Han+ 83].

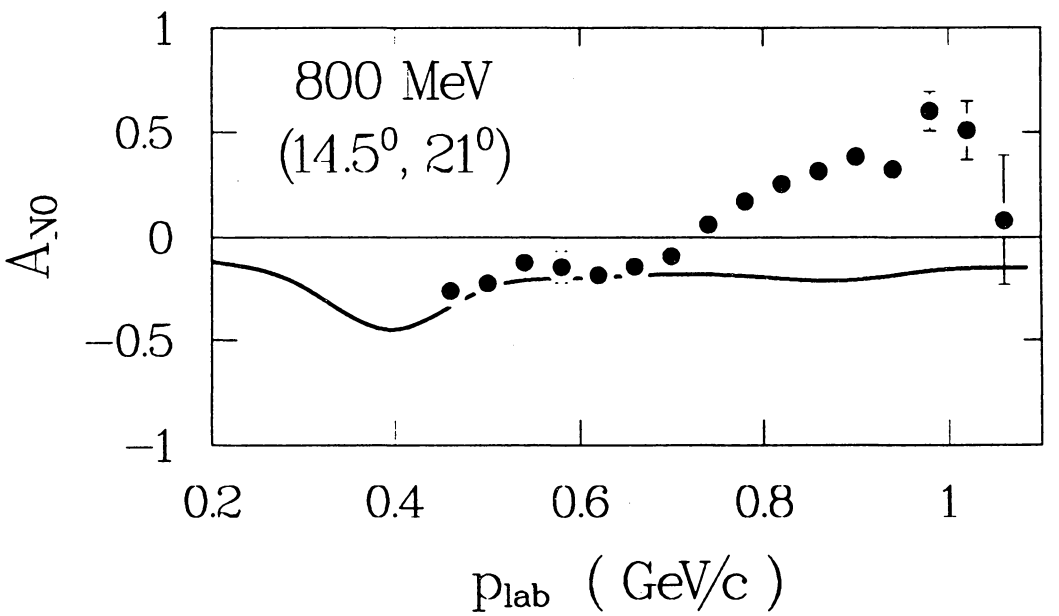

Figure 5.6: Beam asymmetry as predicted by our standard model at $(14.5^0, 21^0)$. Data from Hancock et al. [Han+ 83].

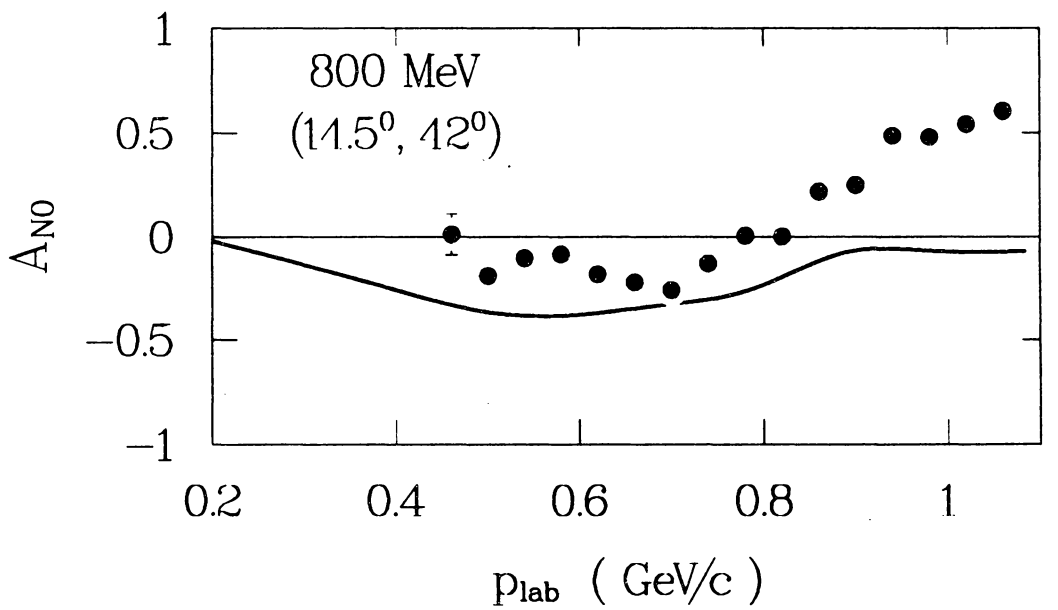

Figure 5.7: **Same as Fig. 5.6 but for** $(14.5^0, 42^0)$**. Data from Hancock et al. [Han+ 83].**

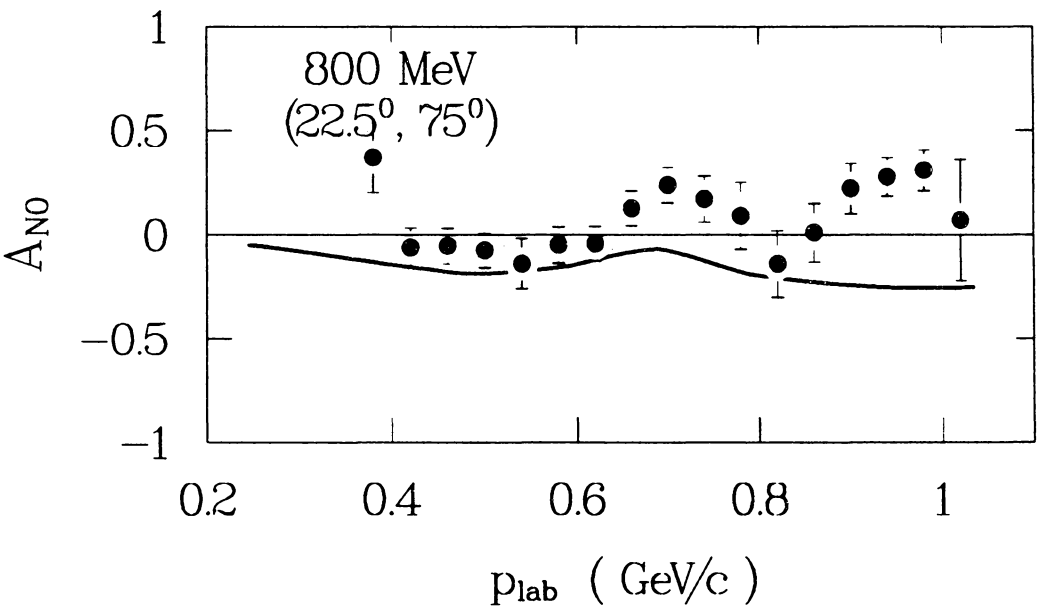

Figure 5.8: Same as Fig. 5.6 but for $(22.5^0, 75^0)$. Data from Hancock et al. [Han+ 83].

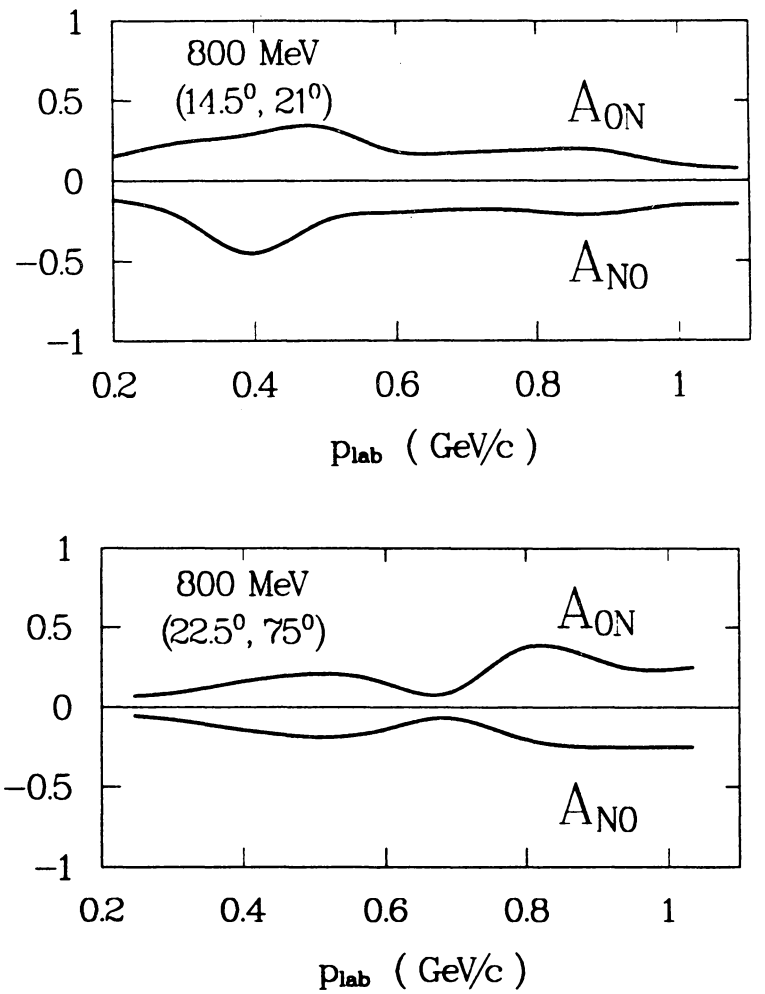

Figure 5.9: Comparison of the beam and target asymmetries for two different kinematical conditions.

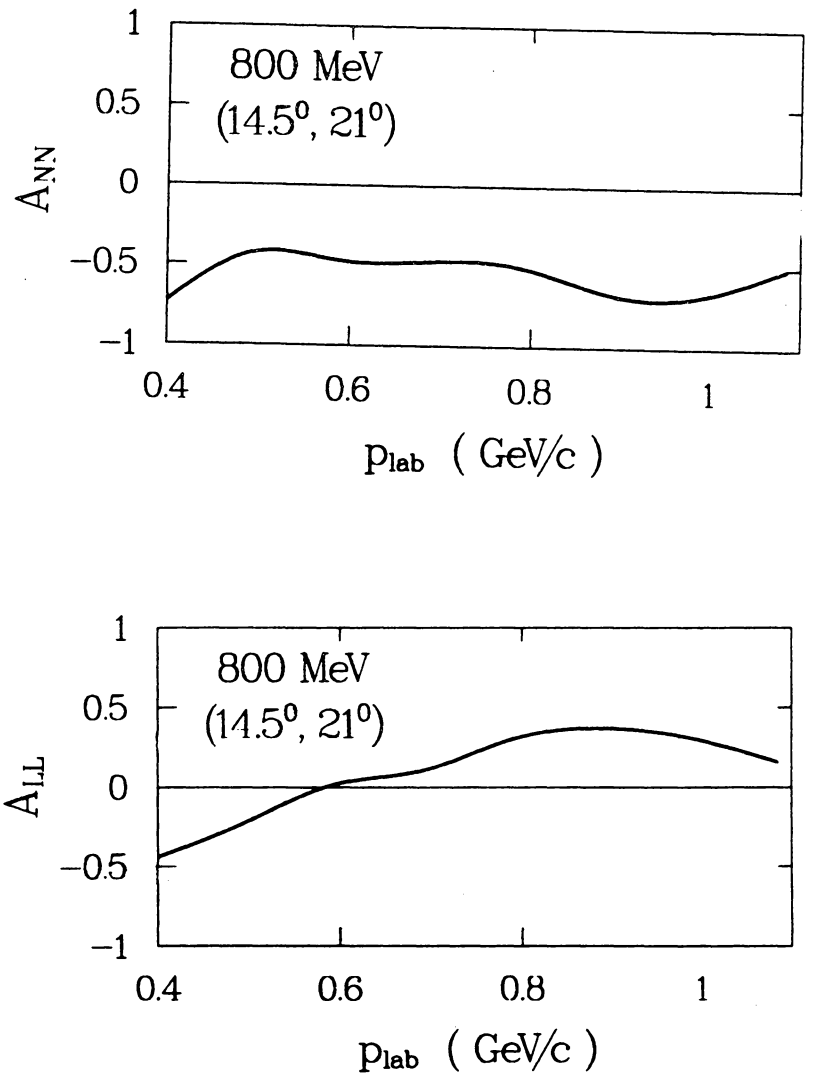

Figure 5.10: Predictions for some spin-spin correlations.

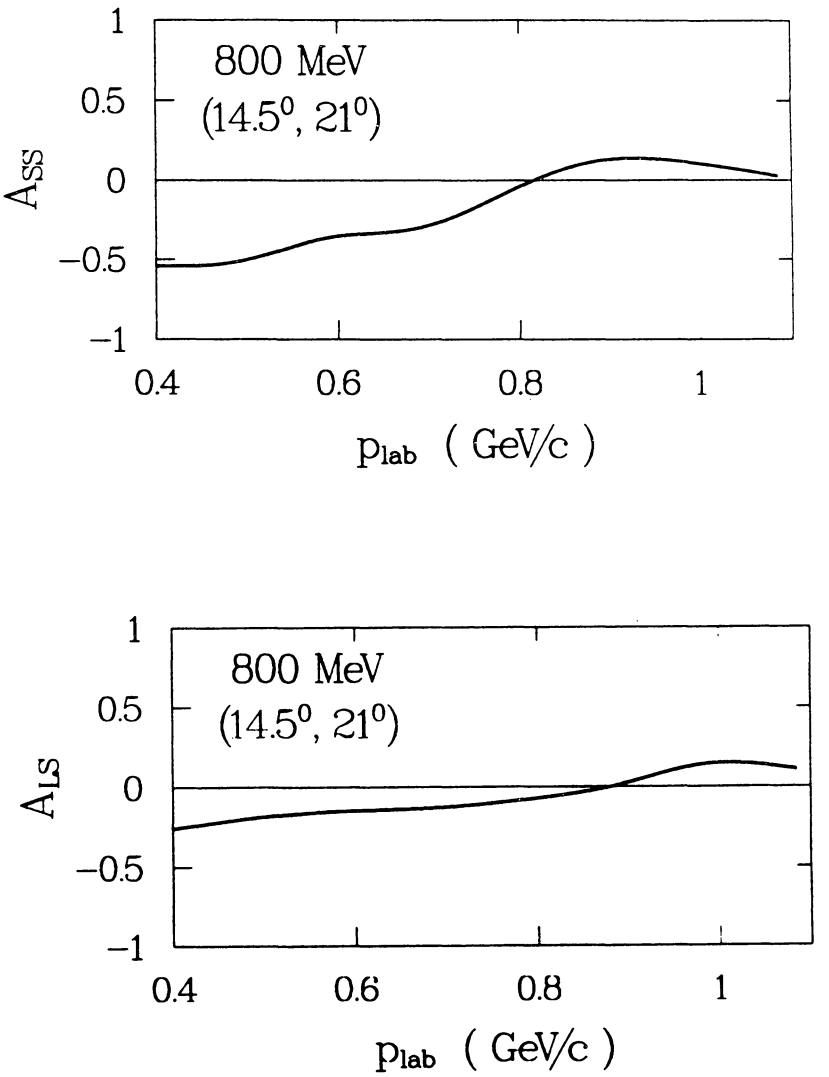

Figure 5.10: continued.

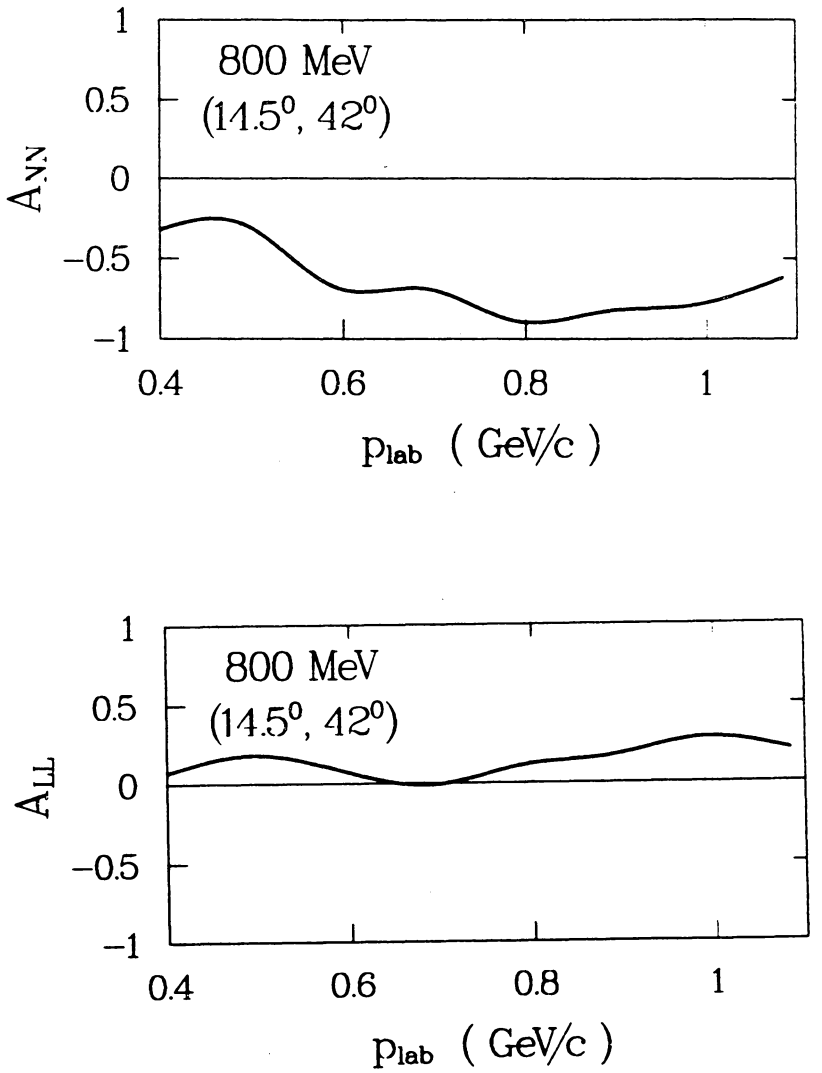

Figure 5.11: Same as Fig. 5.10 but for $(14.5^0, 42^0)$.

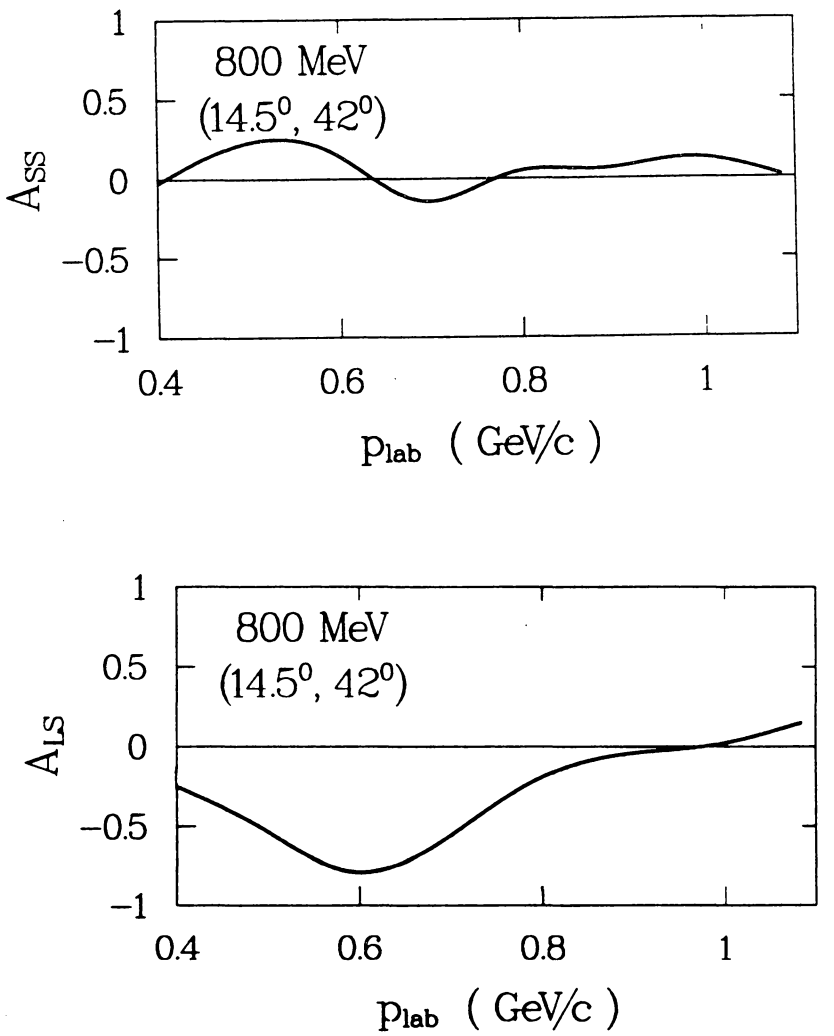

Figure 5.11: continued.

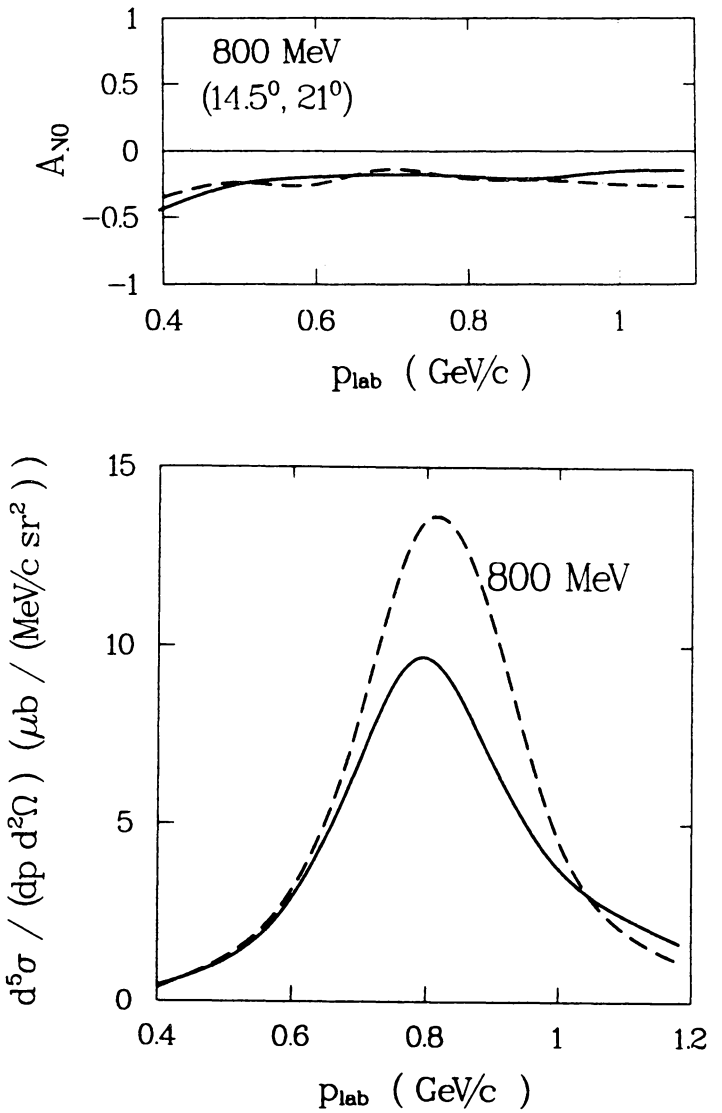

Figure 5.12: Effect on the cross section and the polarization of omitting the lowest partial waves ($J = 0, 1$) at $(14.5^0, 21^0)$ (dashed).

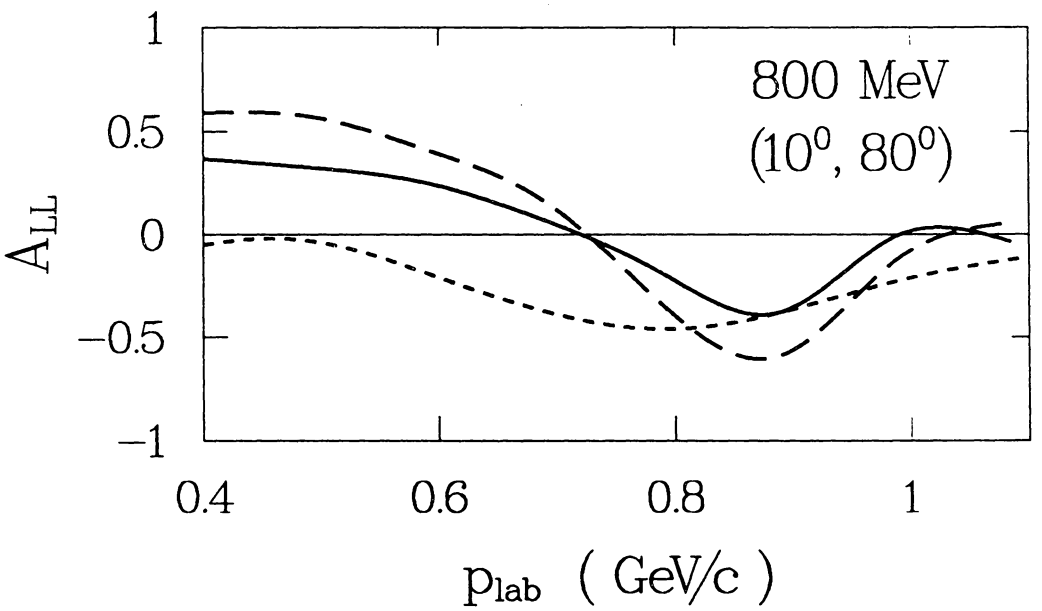

Figure 5.13: Predicted A_{LL} at $(10^0, 80^0)$ (solid) and without the $J = 0, 1$ amplitudes (dashed). The dotted curve represents the full model of Dubach et al. [DKS 82].

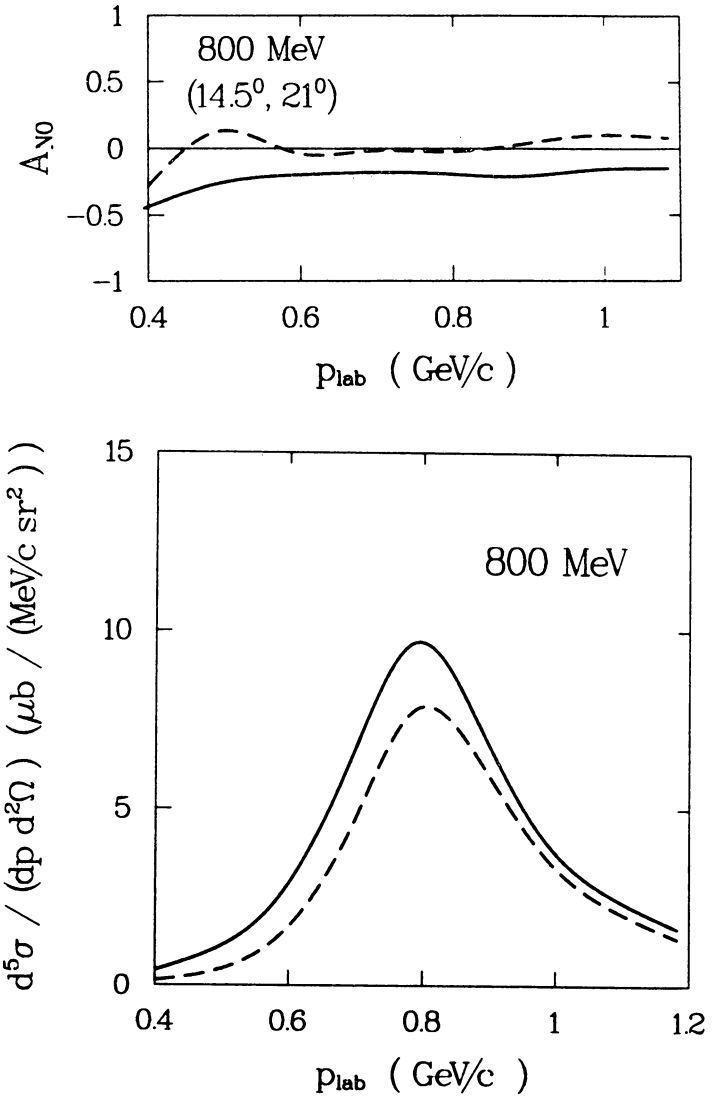

Figure 5.14: Effect on the cross section and polarization at $(14.5^0, 21^0)$ of omitting the $^1D_2$ partial wave (dashed).

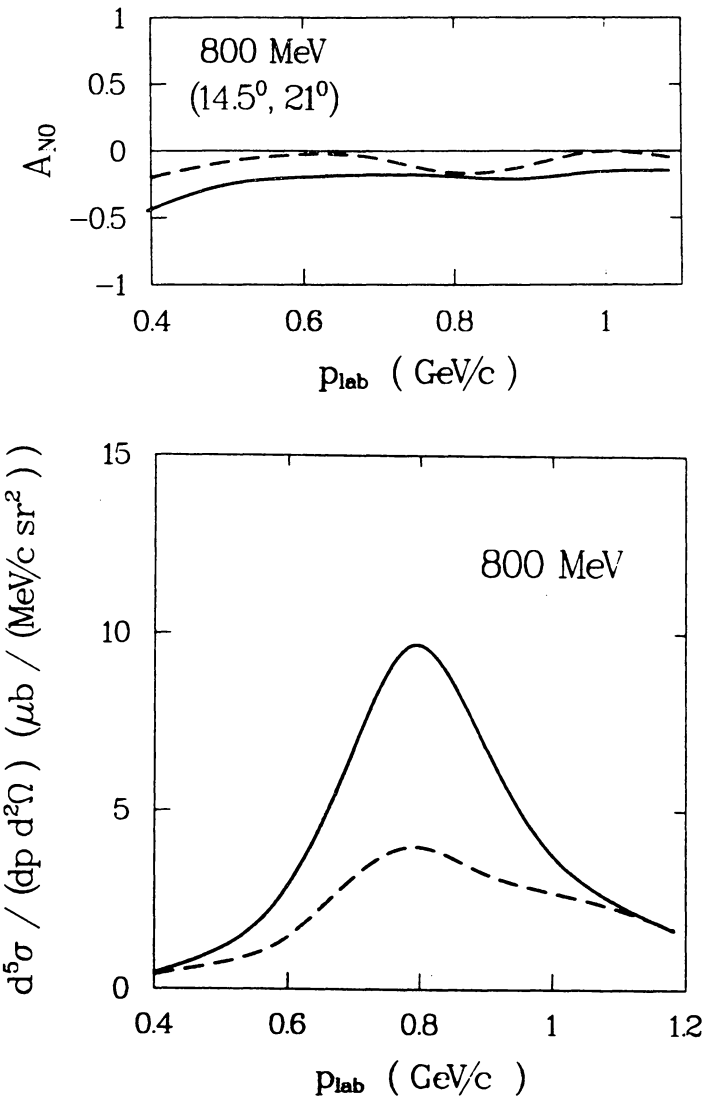

Figure 5.15: **Same as Fig. 5.14 but omitting the $^3F_3$ partial wave (dashed).**

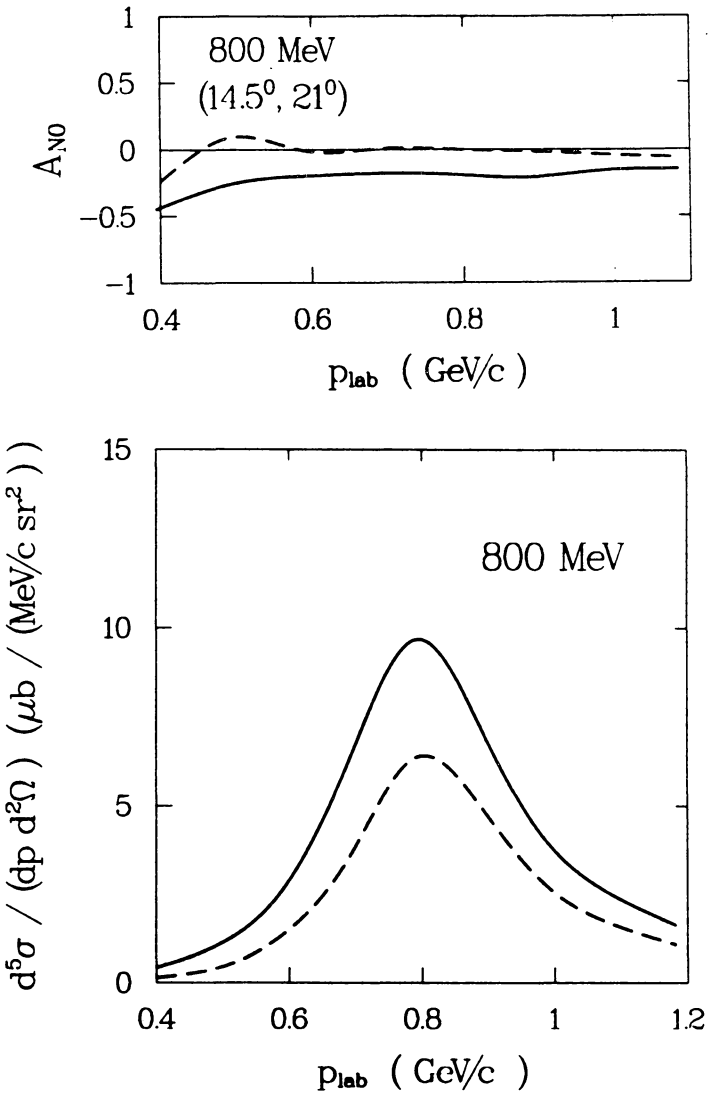

Figure 5.16: Same as Fig. 5.14 but omitting all singlet states (dashed).

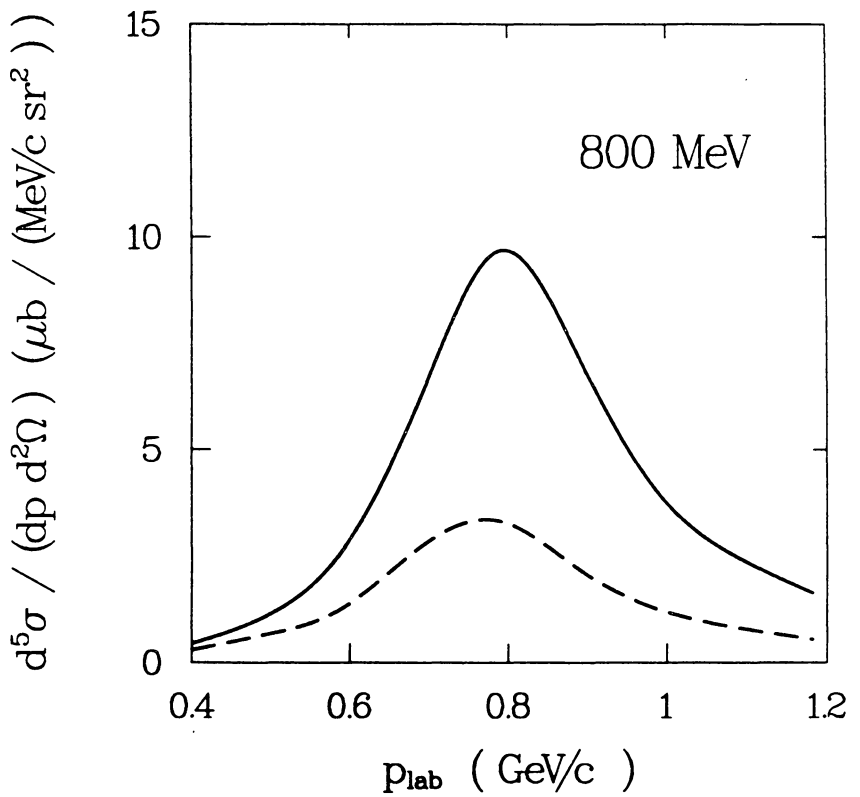

Figure 5.17: Cross section at $(14.5^0, 21^0)$ without the contributions from the triplet states (dashed).

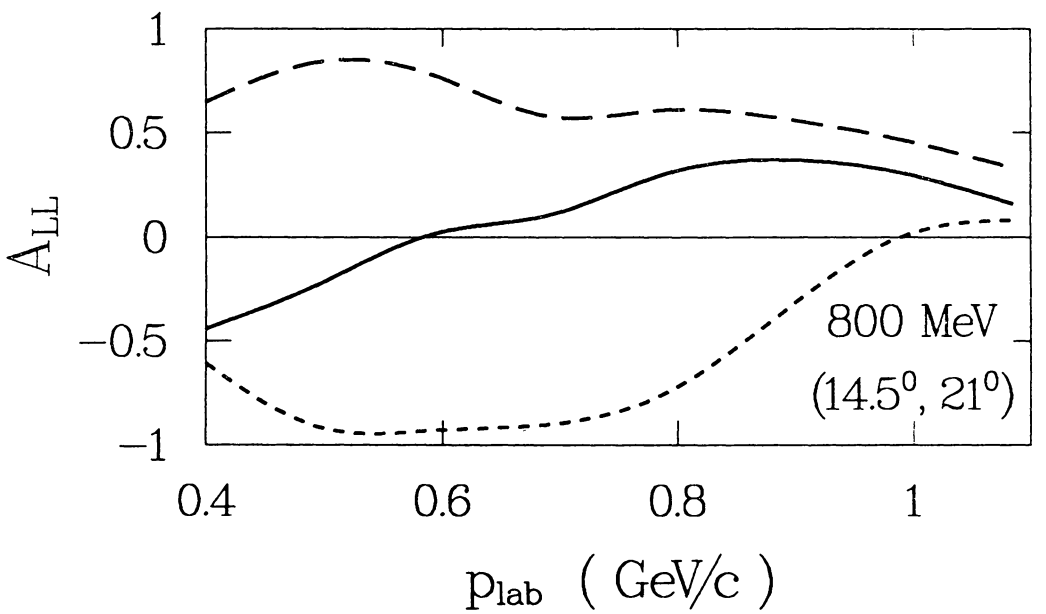

Figure 5.18: **Effect on A_{LL} at $(14.5^0, 21^0)$ of omitting $^1D_2$ (dashed) or $^3F_3$ (dotted).**

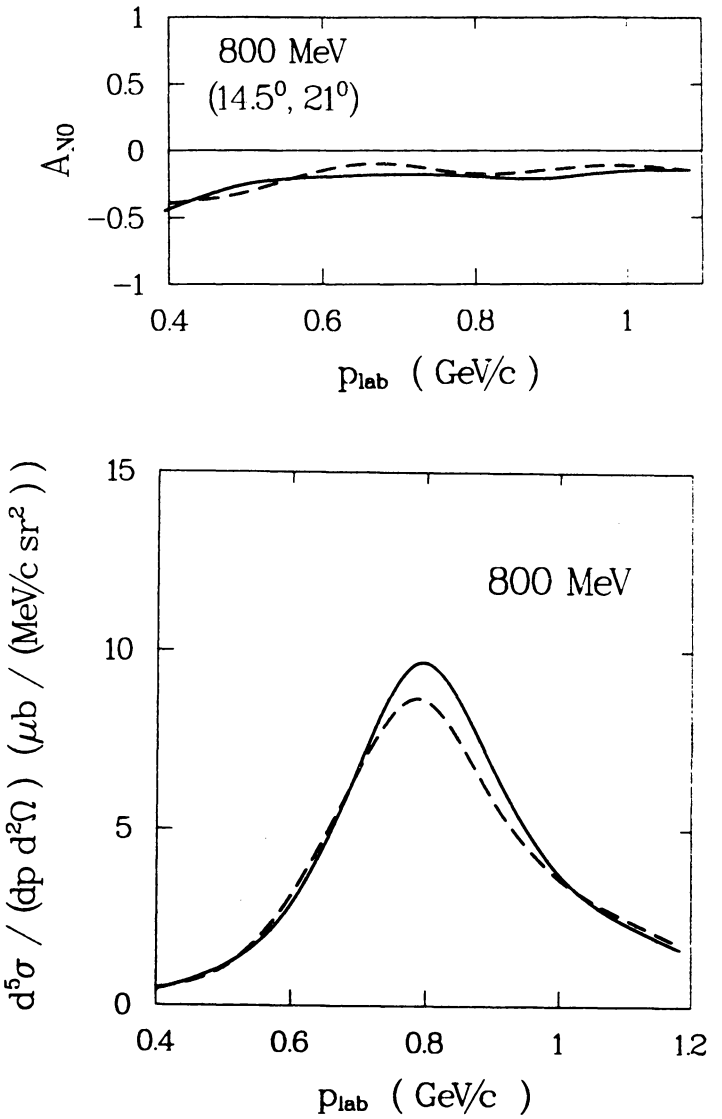

Figure 5.19: Cross section and polarization at $(14.5^0, 21^0)$ with short-range contributions (dashed) and without (solid).

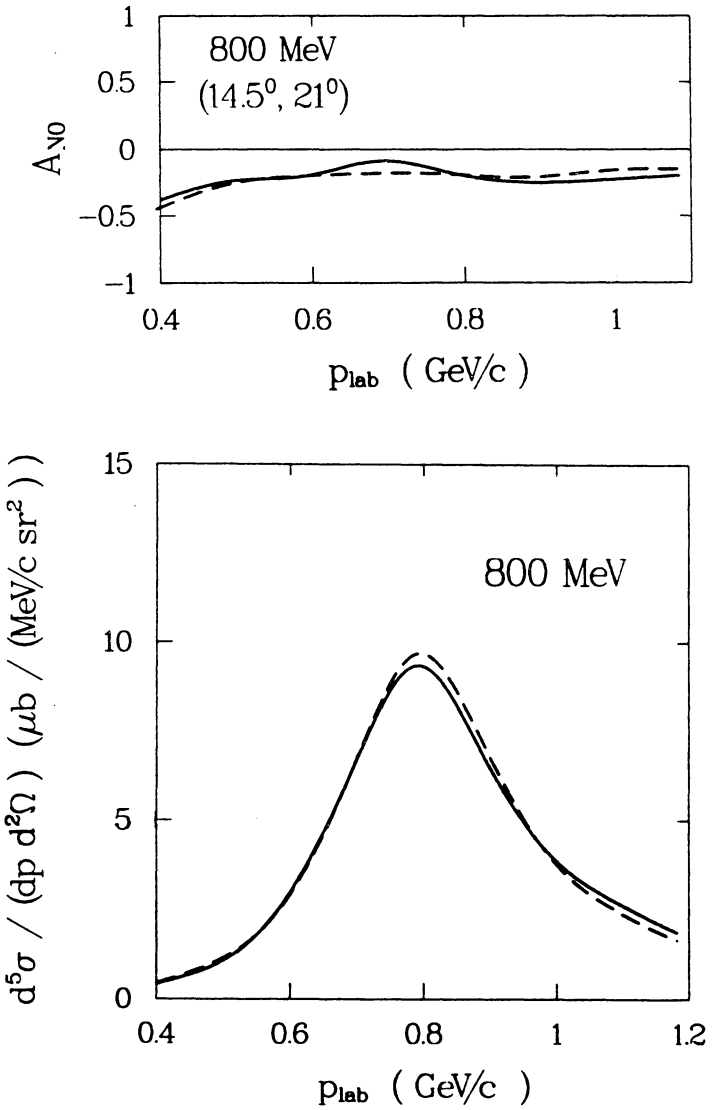

Figure 5.20: Cross section and polarization at $(14.5^0, 21^0)$ with all small πN waves (solid) and without (dashed).

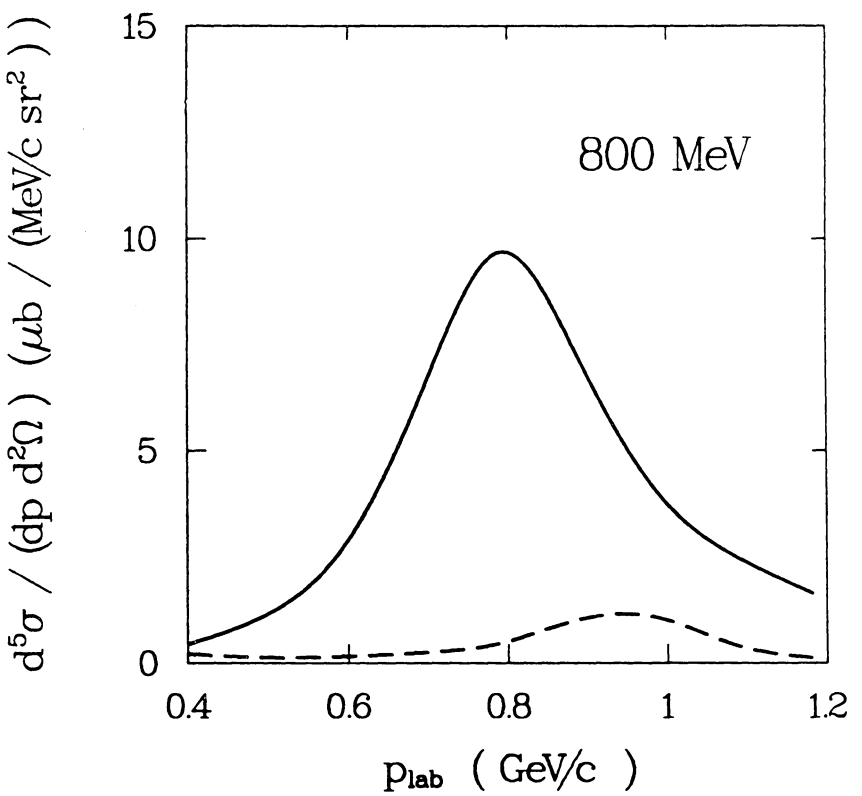

Figure 5.21: Contribution to the cross section at $(14.5^0, 21^0)$ from Δ^+ production only (dashed).

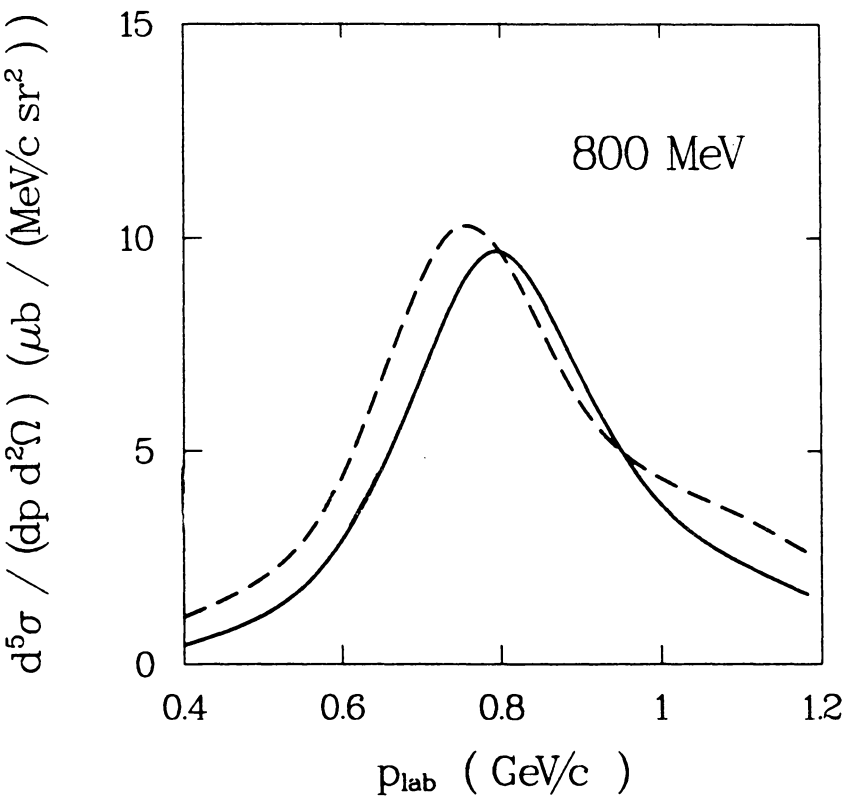

Figure 5.22: **Cross section at $(14.5^0, 21^0)$ as predicted in Born approximation (dashed) compared with the unitary calculation (solid).**

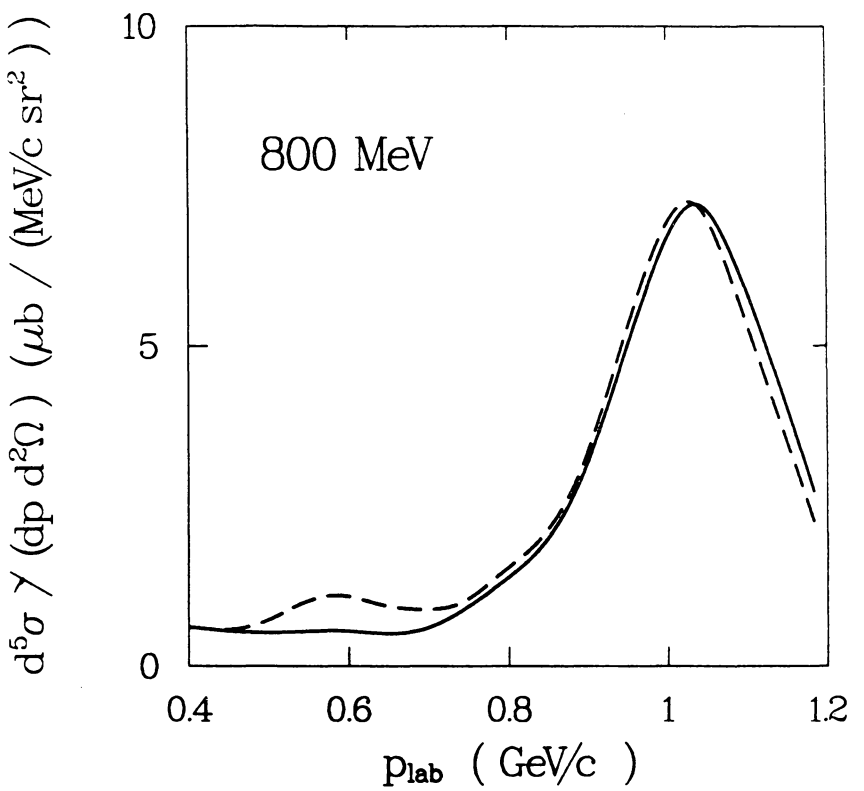

Figure 5.23: **Differential cross section at $(14.5^0, 42^0)$ with the inclusion of the deuteron channel (dashed) and without (solid).**

Chapter 6

Conclusions

In this work, we have been concerned with a relativistic unitary model for the NN and the πNN system. Our model is conventional in the sense that it involves only known mesons and baryons together with effective meson-baryon interactions. In particular, we have examined exclusive π^+ production from the NN system with the goal of further understanding and constraining our theoretical input and achieving some insight to what controls this mechanism.

From an overview of Ch. 4 and 5, it appears that two major aspects of the model need further study: first, the way the inelasticities are taken into account (i.e. the model for the Δ-resonance), and, second, the description of

the short-range forces. As we have seen in Ch. 5, these two issues are rather independent of each other and are not equally important for the break-up channel. Indeed, a definite conclusion we can draw from our results is that short-range effects are not of crucial importance in describing pion production.

We have also seen (Ch. 3) that the low partial waves (in particular the NN P-waves), besides being sensitive to short-range effects, are also strongly affected by the πN input, in particular the P_{11}. A rather puzzling conclusion drawn here is that a quantitative description of the P_{11} πN partial wave seems at variance with a quantitative description of the NN P-waves.

From the analysis performed in Ch. 5 it is clear that the pion production process is dominated by the $^1D_2$ and $^3F_3$ partial waves. In particular, sufficient inelasticity in those two waves guarantees a reasonable prediction of the differential cross section. However, it appears very difficult to obtain correct inelasticity parameters without generating too much attraction in the corresponding real phases.

Among the spin observables, the A_{LL} parameter was found to be strongly dominated by the $^1D_2$ and $^3F_3$ partial waves. A similar conclusion does not

apply to the asymmetry. Notice that A_{LL} depends on amplitudes squared (with opposite sign for singlet and triplet initial states), while A_{N0} is controlled by interferences and hence is phase sensitive. Therefore, it was not possible to isolate the contribution from a particular partial wave. We have already stressed that a major improvement is required for the $^1D_2$ and $^3F_3$ amplitudes; the structure of our predicted observables, and their response to the variations of the model performed in Ch. 5, seem indeed to indicate the need for such an improvement (rather than the need for explicit dibaryon degrees of freedom). The new (unpublished) measurements of the spin correlation parameters for π^+ production, performed at LAMPF by Bugg and collaborators [BUG 88], will be of enormous interest to us. Those observables which have been found very sensitive to $^1D_2$ and $^3F_3$, (for instance A_{LL}), are certainly good candidates for experimental tests on the existence of dibaryon resonances in those partial waves.

Since there is still some latitude in the model for how the Δ-resonance is treated, one facet of the current research of our group [MF 88] is devoted to whether some of the problems can be solved through an improved model for P_{33} (keeping in mind a realistic description of the P_{11}). In this respect a possible solution has been found in the use of a higher rank potential for the

P_{33}. While this would probably not settle every open question, it may be an indication that our present difficulties in describing inelastic processes are due to limitations of the models rather than to a general failure of meson-baryon theory to explain the NN data above pion production threshold.

We emphasize that no model is, so far, in better than qualitative agreement with experiment for the $NN \rightarrow \pi NN$ reaction. In a study of the model dependence of this process [Dub+ 86], the major source of the differences has been identified as due to the $NN(^1D_2) \rightarrow N\Delta(^5S_2)$ transition. As already mentioned, one way to improve this transition is to exploit modifications of the $\pi N\Delta$ vertex. Also, the effect of the two-body NN interaction should be carefully studied (see last section of Ch. 5).

At the present time, it appears reasonable to attribute the problems to a large latitude left in the meson-baryon models. Other limitations in today's models, besides the description of the πN input, are more 'intrinsic'. For instance, the ways we implement relativistic kinematics and the forms of the meson propagator (see Ch. 2) do introduce a certain arbitrariness.

This work, by extending the model to the break-up channel, has basically set up the tools for a parallel or unified study of the two- and three-body NN reactions. This type of study will present a stronger constraint

on the model and may help in deciding what aspects of the dynamics are most sensitive to the various components of the theory.

Bibliography

[Aar 77] R. Aaron, in *Modern Three-Hadron Physics* (A. W. Thomas, ed.), ch. 5, Springer, Berlin (1977).

[AAY 68] R. Aaron, R. D. Amado, and J. E. Young, *Phys. Rev.* **174**, 2022 (1968).

[AM 83] Y. Avishai and T. Mizutani, *Phys. Rev. C* **27**, 312 (1983).

[Arn+ 83] R. A. Arndt et al., *Phys. Rev. D* **28**, 97 (1983).

[Aue+ 77] I. P. Auer et al., *Phys. Lett.* **67B**, 113; **70B**, 475 (1977).

[BA 81] B. Blankleider and I. R. Afnan, *Phys. Rev. C* **23**, 1384; *C* **24**, 1572 (1981).

[BS 66] R. Blankenbecler and R. Sugar, *Phys. Rev.* **142**, 1051 (1966).

[Bug 88] D. V. Bugg, Dibaryons and Amplitudes for $NN \to NN\pi$, *Contribution to the Rensselaer Conference on Excited Baryons* (1988).

[Bys+ 84] J. Bystricky *et al.*, *Nuovo Cim.* **82A**, 385 (1984).

[BW 75] G. E. Brown and W. Weise, *Phys. Reports* **C22**, 281 (1975).

[DKS 82] J. Dubach, W. M. Kloet, and R. R. Silbar, *J. Phys. G* **8**, 475 (1982).

[DKS 86] J. Dubach, W. M. Kloet, and R. R. Silbar, *Phys. Rec. C* **33**, 373 (1986).

[DKS 87] J. Dubach, W. M. Kloet, and R. R. Silbar, *Nucl. Phys.* **A466**, 573 (1987).

[Dub+ 86] J. Dubach *et al.*, *Phys. Rev. C* **34**, 944 (1986).

[Fad 61] L. D. Faddeev, *JETP (Sov. Phys.)* **12**, 1014 (1961).

[Gro 82] F. Gross, *Phys. Rev. C* **26**, 2203 (1982).

[Han+ 83] A. D. Hancock *et al.*, *Phys. Rev. C* **27**, 2742 (1983).

[Hid+ 77] H. Hidaka *et al.*, *Phys. Lett.* **70B**, 479 (1977).

[HM 75] K. Holinde and R. Machleidt, *Nucl. Phys.* **A247**, 495 (1975).

[HM 87] B. ter Haar and R. Malfliet, *Phys. Reports* **149**, 207 (1987).

[KS 80] W. M. Kloet and R. R. Silbar, *Nucl. Phys.* **A338**, 281 (1980).

[KS 81] W. M. Kloet and R. R. Silbar, *Nucl. Phys.* **A364**, 346 (1981).

[KTS 81] W. M. Kloet, J. A. Tjon, and R. R. Silbar, *Phys. Lett.* **99B**, 80 (1981).

[Lac+ 80] M. Lacombe *et al.*, *Phys. Rev. C* **21**, 861 (1980).

[Lam+ 87] G. H. Lamot *et al.*, *Phys. Rev C* **35**, 239 (1987).

[Lee 84] T.-S. H. Lee, *Phys. Rev. C* **29**, 195 (1984).

[Lom 82] E. L. Lomon, *Phys. Rev. D* **26**, 576 (1982).

[Mac 88] R. Machleidt, *Adv. Nucl. Phys.* **19**, in press.

[MF 88] T. Mizutani and C. Fayard, priv. communication.

[MHE 87] R. Machleidt *et al.*, *Phys. Reports* **149**, 1 (1987).

[Miz+ 81] T. Mizutani *et al.*, *Phys. Rev. C* **24**, 2633 (1981).

[ML 86] A. Matsuyama and T.-S. H. Lee, *Phys. Rev. C* **34**, 1900 (1986).

[Nak 69] N. Nakanishi, *Prog. Theor. Phys. (Kyoto), Supplement* **43**, 1 (1969).

[PDG 84] Particle Data Group, *Rev. Mod. Phys.* **56**, S1 (1984).

[Per 84] J. L. Perrot, thesis, University of Lyon Report LYCEN 8409 (1984).

[PSZ 87] H. Pöpping, P. U. Sauer, and Zhan, Xi-Zhen, *Nucl. Phys.* **A474**, 557 (1987).

[Rei 84] M. J. Reiner, *Ann. Phys. (N. Y.)* **154**, 24 (1984).

[RT 77] A. S. Rinat and A. W. Thomas, *Nucl. Phys.* **A282**, 365 (1977).

[SB 51] E. E. Salpeter and H. A. Bethe, *Phys. Rev.* **84**, 1232 (1951).

[Sil 88] R. R. Silbar, priv. communication.

[SZM 79] K. Schwarz, H. F. K. Zingl, and L. Mathelitsch, *Phys. Lett.* **83B**, 297 (1979).

[Ued 86a] T. Ueda, *Phys. Lett.* **175B**, 19 (1986).

[Ued 86b] T. Ueda, *Prog. Theor. Phys.* **76**, 729 (1986).

[Wic+ 86] A. B. Wicklund et al., *Phys. Rev. D* **34**, 19 (1986).

[WMA 75] R. M. Woloshyn, E. J. Moniz, and R. Aaron, *Phys. Rev. C* **12**, 909 (1975).

Appendix A

Numerical Techniques

When solving numerically Eq. (2.4), one is faced with the problem of handling various types of singularities. The singularity of the propagator (arising from the energy denominator in Eq. (2.8)) does not present particular problems: numerical stability is obtained with 32 mesh points for the integration and the use of standard subtraction techniques.

The singularities of the Born terms, coming from the energy denominator in Eq. (2.10), require a more careful treatment.

First, it must be mentioned that, when one is interested in the on-shell amplitude only, the integral equation can be solved easily by standard contour rotation techniques. The half-off-shell matrix elements, calculated

in the complex plane (i. e. for complex momenta), are then integrated to provide the on-shell amplitude; in this way, no usable information about the off-shell T-matrix is left. Half off-shell isobar amplitudes as a function of physical (i. e. real) momenta are, however, essential in our case, as they feed the break-up calculation (see Section 5.2). We must therefore remain on the real axis and directly face each singularity.

When inverting the (LSJ) expansion of the Born terms (an expression analogous to Eq. (5.4)), the resulting (LSJ) projections can be schematically written (we are first considering the case of pion exchange) as

$$B_{LSJ}(p',p) = \int_{-1}^{+1} dz \frac{f(z)}{W^2 - (E_{\mathbf{p}'} + E_{\mathbf{p}} + \omega_{\mathbf{p}+\mathbf{p}'})^2} \tag{A.1}$$

with $z = \hat{\mathbf{p}} \cdot \hat{\mathbf{p}}'$ (see Eq. (2.10) and Fig. 2.2 for notation and particle labels). We have incorporated in $f(z)$ any other function of z, besides the energy denominator, as well as expansion coefficients, irrelevant for the present discussion. The integral in Eq. (A.1) has a pole whenever $\mathbf{p}$ and $\mathbf{p}'$ satisfy

$$W = \sqrt{s} = E_{\mathbf{p}} + E_{\mathbf{p}'} + \omega_{\mathbf{p}+\mathbf{p}'}. \tag{A.2}$$

When $B_{LSJ}(p',p)$, after integration over z, is seen as a function of the momenta, this singularity will give a cut and branch point structure typical of

all three-body problems at energies above break-up threshold. This has to be carefully considered when performing the final (momentum) integration. First, we must deal with the integral in Eq. (A.1), which is done by closely following Kloet and Silbar [KS 80]. For values of $\mathbf{p}$ and $\mathbf{p}'$ such that the denominator in Eq. (A.1) does not vanish, the integration is straightforward and is performed by using 16 Gaussian points in the interval $[-1,+1]$.

In those cases when the pole is present, defining the new integration variable [KS 80]

$$s_z = (E_{\mathbf{p}} + E_{\mathbf{p}'} + \omega_{\mathbf{p}+\mathbf{p}'})^2 \,, \tag{A.3}$$

we can rewrite Eq. (A.1) in a form which is convenient for the purposes of regularization, namely

$$B_{LSJ}(p',p) = \int_{s_1}^{s_2} \frac{F(s_z)}{s - s_z} ds_z \tag{A.4}$$

with s_1 and s_2 the values of the new integration variable corresponding to $z = -1$ and $+1$, respectively. Obviously, the singularity occurs for $\mathbf{p}$ and $\mathbf{p}'$ such that $s_1 \leq s \leq s_2$. In these cases, Eq. (A.4) becomes, after regularization,

$$B_{LSJ}(p',p) = \int_{s_1}^{s_2} \frac{F(s_z) - F(s)}{s - s_z} ds_z + F(s) ln|\frac{s_2 - s}{s_1 - s}| - i\pi F(s). \tag{A.5}$$

The principal value integral in Eq. (A.5) is computed with 16 Gaussian points chosen symmetrically about the singularity.

We consider next the Born projections as a function of the momenta.

For a given total C.M. energy above break-up threshold ($W > 2m + \mu$), production singularities occur when the invariant masses of the initial and final isobars satisfy

$$\begin{aligned} \sigma_{\mathbf{p}'} &= W^2 - 2WE_{\mathbf{p}'} + m^2 \geq (m+\mu)^2 \\ \sigma_{\mathbf{p}} &= W^2 - 2WE_{\mathbf{p}} + m^2 \geq (m+\mu)^2. \end{aligned} \tag{A.6}$$

The above implies $E_{\mathbf{p}'} < E_b, E_{\mathbf{p}} < E_b$, with

$$E_b = (W^2 - 2m\mu - \mu^2)/2W \tag{A.7}$$

defining the limits of the production region.

In the following, $p(p')$ is the magnitude of the three-momentum $\mathbf{p}(\mathbf{p}')$. When the singularity condition Eq. (A.2) is solved for p' as a function of p, we obtain

$$p' = \frac{-p'Az \pm \sqrt{\alpha^2[A^2 + 4m^2(p^2z^2 - \alpha^2)]}}{2(\alpha^2 - p^2z^2)} \tag{A.8}$$

with $\alpha^2 = \sigma_p^2 + p^2$ and $A = \sigma_p + m^2 - \mu^2$.

The boundaries of the singularity domain are defined by $z = \pm 1$, there-

fore

$$p' = \frac{\pm p'A \pm \sqrt{\alpha^2[A^2 + 4m^2(p^2 - \alpha^2)]}}{2(\alpha^2 - p^2)}. \qquad (A.9)$$

In the physical region, where both p and p' are positive, the structure of the production singularity branch points is shown in Fig. A.1, for a laboratory energy of 800 MeV (corresponding to a total C.M. energy of 2242 MeV).

When integrating the equation over p' for a given p (i. e. moving upward in the vertical direction, see Fig. A.1), one encounters two singular points (A and B) on the edges of the bell shaped curve. The complication arises from the fact that, for each p, different singular points are encountered; therefore, for each p, we must locate the corresponding singularities and choose the integration points accordingly. The general technique [KS 80] consists in subdividing the integration path within the 'production box' (delimited by P_b, which is the momentum corresponding to E_b, Eq. (A.7)) such that the points are symmetrically distributed about the singularities. In Fig. A.2 we show the cases which typically occur. Case (a) corresponds to the situation when the singularities (A and B) are far from each other and from the edges of the production box. We then subdivide the interval $[O, P_b]$ as in Fig. A.2a and we take 2 Gaussian points in each of the small intervals about A and B, and 4 points in each of the other intervals (OC,

DE, FP_b). Within this case, further selections are made; for instance, if A and B are much closer to each other than to the edge points, less mesh may be needed in the middle interval DE, where we take 2 points, while 4 are chosen in FP_b and 6 in OC. Actually, even more delicate situations can occur. For example, it can happen that A and B are so close to each other that it is practically impossible to surround them with symmetrical intervals as in Fig. A.2*a*. This type of problem can be solved rather empirically by keeping control on the density of the points p so as to avoid very critical cases and, therefore, too many sub-selections. Actually, we take 8 points for p in the production region, distributed as follows (see Fig. A.1): 4 in $0P_1$, 2 in P_1P_2 and 2 in P_2P_b.

Cases (*b*) and (*c*) in Fig. A.2 occur when either one of the singularities is very close to the edges. For case (*b*), we take again 2 points in each of small the intervals about A and B, 4 points in OC and 8 in the largest (DE).

For case (*c*), we take 8 points in CD, 4 in EP_b and 2 in each of the smaller intervals. For all cases above, we have then chosen 20 integration points in the region OP_b.

Outside the production region, the singularity arising from the nucleon

pole (or the πN two-body sub-system having a bound state at $\sigma = m^2$, see Eq. (2.9)) is always present, even for energies below break-up threshold. The pole is treated with subtraction, and 12 points are used outside the production region for both p and p', giving a total of 32 (20+12) integration mesh and 20 (8+12) values of p for which the equation is solved (actually 21, as the on-shell NN momentum is included in the set p to obtain the on-shell $NN \to NN$ amplitude.)

As we have seen, the above choices have been dictated by the position of the singularities typical of the pion exchange Born terms. A completely analogous discussion applies to the nucleon exchange case (when either the initial or final state is a πd channel), except for the fact that the singularities are numerically different. In fact, the problem can be handled in an exactly parallel way, if one starts by imposing the appropriate singularity conditions for the nucleon exchange case corresponding to Eq. A.2 and A.6.

For the transition $NN(N\Delta) \to \pi d$, the final 'isobar' is the deuteron with momentum $\mathbf{p}'$ and the exchanged particle is now a nucleon with momentum $\mathbf{p} + \mathbf{p}'$. The relation corresponding to Eq. (A.2) will now be

$$W = \sqrt{s} = E_{\mathbf{p}} + \omega_{\mathbf{p}'} + E_{\mathbf{p}+\mathbf{p}'} \tag{A.10}$$

with the necessary condition for the break-up singularity being

$$\begin{aligned} \sigma_{\mathbf{p}'} &= (W - \omega_{\mathbf{p}'})^2 - \mathbf{p}'^2 \geq (2m)^2 \\ \sigma_{\mathbf{p}} &= (W - E_{\mathbf{p}})^2 - \mathbf{p}^2 \geq (m + \mu)^2 \end{aligned} \tag{A.11}$$

Solving the singularity condition for the πd channel momentum as a function of the $NN(N\Delta)$ momentum, or vice versa, gives the branch point structures shown in Fig. A.3 and A.4 respectively. The point P_c in the figures is the maximum critical momentum of the πd channel for which singularities exist, and it is given by the condition

$$\sigma_{P_c} = W^2 - 2W\omega_{P_c} + \mu^2 = 4m^2 \tag{A.12}$$

which implies

$$\omega_{P_c} = \frac{W^2 - 4m^2 + \mu^2}{2W} \tag{A.13}$$

and

$$P_c = \sqrt{\omega_{P_c}^2 - \mu^2} \tag{A.14}$$

The non-symmetric structure of the nucleon exchange singularities under interchange of initial and final states implies that two different sets of integration points must be used just for the $NN \leftrightarrow \pi d$ case. In other words, when the πd channel appears as an intermediate state (and therefore

must be integrated over), the curve in Fig. A.3 must be used to locate the singularities and select 'moving mesh' p' as a function of p. The same holds for Fig. A.4 in the case of integrated $NN(N\Delta)$ momentum and initial πd state. In both cases, the criteria we have used for subdividing the integration path with respect to the position of the singularities are identical to those explained for the pion exchange case (and therefore we will not repeat the discussion here); the same number of mesh points is used, namely 32 overall on the vertical axis and 21 on the horizontal.

The contributions to the amplitude from pion exchange, $\pi d \to NN$ and $NN \to \pi d$, must then be computed separately, since they require different choices of off-shell momenta. As a last step, a cubic spline interpolation is used to compute all the contributions in one set of points, so that they can be summed up.

The equation is finally solved by the Padé approximant technique, which works schematically as follows. Suppressing channel indices, the Neumann series for the T-matrix is

$$T_\lambda = T^{(0)} + \lambda T^{(1)} + \lambda^2 T^{(2)} + ... \qquad \text{(A.15)}$$

where $T^{(0)} = B$, $T^{(1)} = \int BRB$, $T^{(2)} = \int BRT^{(1)}$ and so on. The Padé

approximant for $T = T_{\lambda=1}$ of degree $[M, N]$ is a ratio of two polynomials in λ of degrees M and N respectively, evaluated at $\lambda = 1$:

$$T[M,N] = [P_M(\lambda)/Q_N(\lambda)]_{\lambda=1} \tag{A.16}$$

The coefficients of P_M and Q_N are chosen so that the first $M+N+1$ terms of the power series expansion of $T_\lambda[M,N]$ agree, to that order, with the Neumann series.

In our case, a good convergence is achieved with $M = N = 5$ up to $J = 3$. For higher angular momentum, only a first order iteration was needed, i. e.

$$T = B + \int BRB \tag{A.17}$$

The technique described above for handling the break-up singularities is certainly careful, but also extremely involved. It must be mentioned, however, that such a careful approach may not always be needed, according to the outcome of our many numerical tests. Interestingly, we were able to achieve stability by simply integrating through the singularities, with no particular treatment of them except for increasing the overall density of points in the production region. At a laboratory energy of 800 MeV (which is our 'working energy'), stability was reached with 24 points in

the singularity region (and 41 overall). Notice that, at 800 MeV, the limit of the production box is given, in the pion exchange case, by P_b =2.47 fm^{-1}; this density (24 points in $[0, P_b]$) is therefore rather high, considering that, in absence of singularities (for instance when contour rotation is applied), 24 points are usually sufficient in the whole range $[0, \infty]$. The fact that stability can be achieved at a certain (energy-dependent) density does, indeed, have an analytical justification: after all, we are dealing with quasi-logaritmic singularities and, therefore, formally speaking integrable (unlike, for instance, a pole.) Numerically, this means that it is possible to 'pick up' all the variations of the function with appropriate density (it is not self-evident, however, that this will happen at a reasonable density of points, which is a major constraint for the calculation to be manageable in practice.)

At energies up to 800 MeV, by integrating directly through the singularities, we were able to reproduce our previous results (obtained with the more careful approach described above) within 2% in the worst case. Obviously, this is not a true alternative technique, but just the exploitation of an observed numerical fact, which may be of some interest to the reader who is faced with a similar problem. The safe approach of circumventing

the singularities is still indispensable for a reliable calculation at energies as high as the model allows.

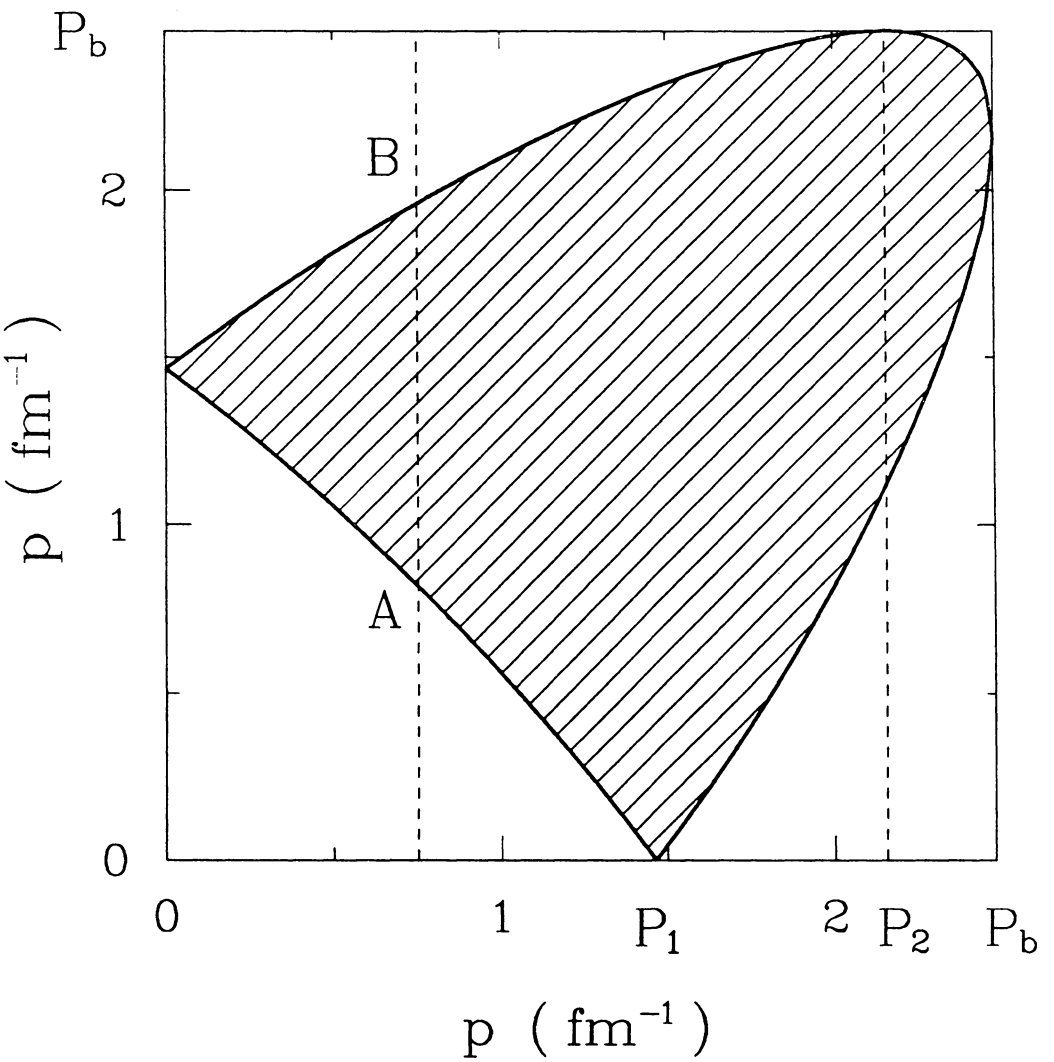

Figure A.1: Structure of the production singularity branch points for the pion-exchange case at a laboratory energy of 800 MeV.

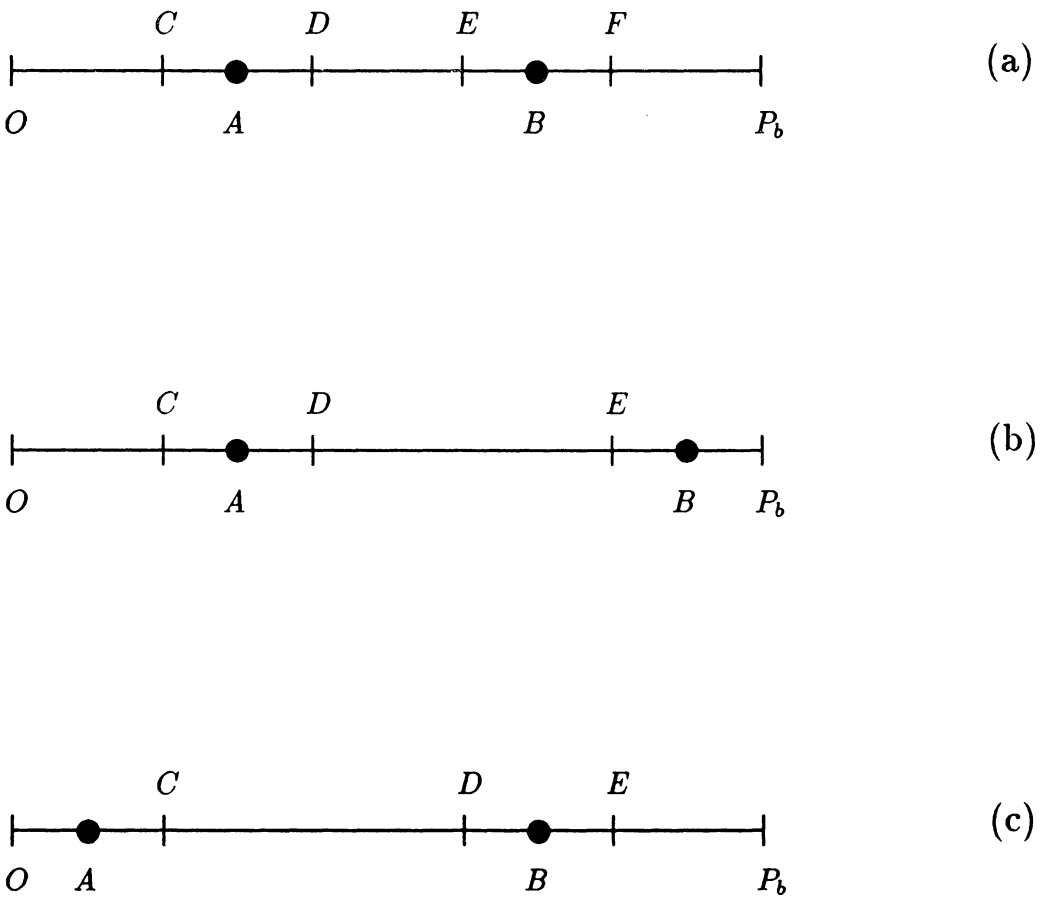

Figure A.2: Subdivisions of the integration paths within the production region for various positions of the singularities.

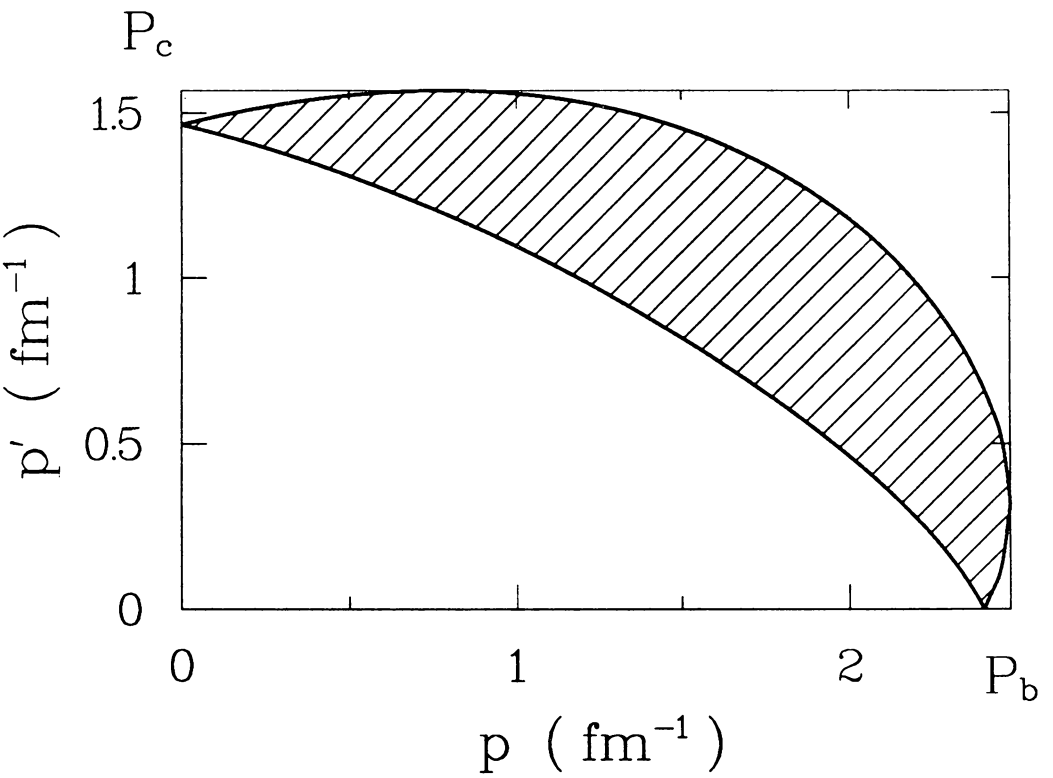

Figure A.3: Structure of the production singularity branch points for the nucleon-exchange case at a laboratory energy of 800 MeV. The πd channel momentum is on the vertical axis.

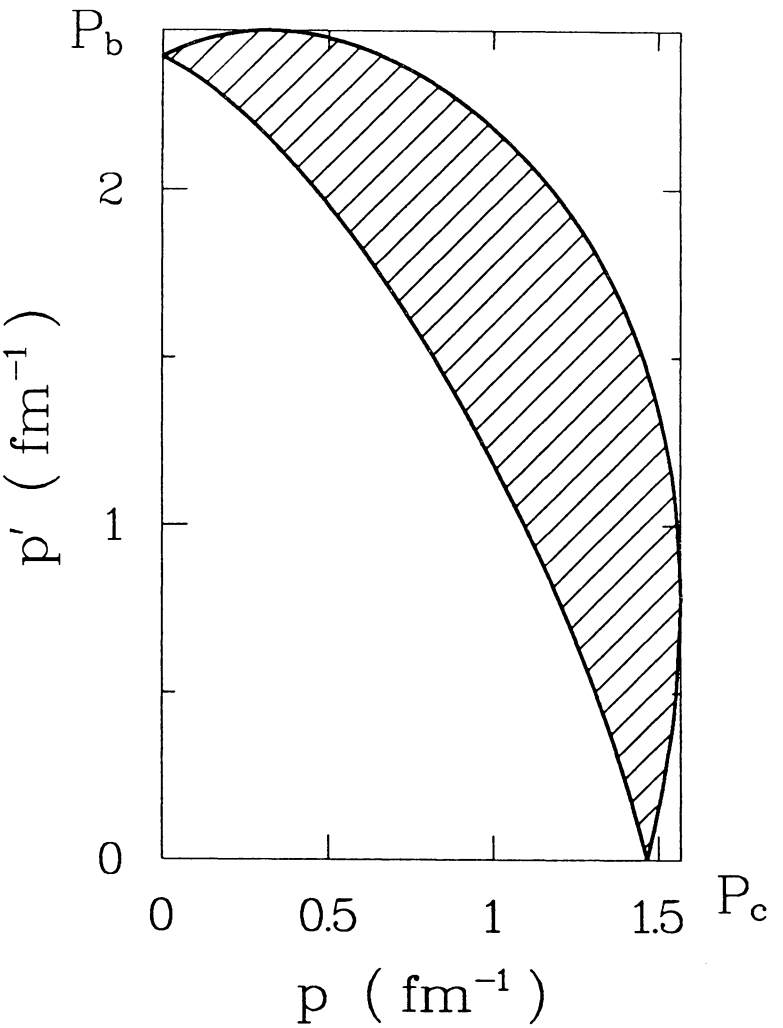

Figure A.4: Same as in Fig. A.3, but with the πd channel momentum on the horizontal axis.

Appendix B

Some Technical Details

We explain here how the observables shown in Section 5.3 are calculated.

As already outlined in Section 5.2 the procedure is as follows: for assigned proton final momentum (p_p) and assigned proton and pion final directions (θ_p and θ_π), we first solve the energy-momentum conservation equations for unmeasured kinematical quantities. As a second step, a boost from the laboratory frame to the C.M. frame is performed; this allows to compute the $2 \rightarrow 3$ body amplitude (see Fig. 5.1) using the appropriate C.M. quantities (i. e. corresponding to the experimental conditions). As a Lorentz invariant, the amplitude will then be valid in any frame.

The boost parameters are

$$\begin{aligned} \beta &= \frac{p_{in}}{E_{in}+m} \\ \gamma &= (1-\beta^2)^{-1/2} \end{aligned} \tag{B.1}$$

where $E_{in} = E_{lab} + m$ is the incident energy, and p_{in} the corresponding momentum.

The $2 \rightarrow 3$ body amplitude has been shown in Ch. 5 to be

$$T_{23} = \langle m_1', m_2', \mathbf{p}_1, \mathbf{p}_2 | T | \mathbf{p}, m_1, m_2 \rangle = \sum_{m_\alpha} \langle \mathbf{p}_1, m_1' | \alpha, -\mathbf{p}_3, m_\alpha' \rangle R(\sigma_{p_3}) T_{N\alpha} \tag{B.2}$$

where the first factor at the left-hand side is the isobar dissociation vertex given by Eq. (5.1), R is the isobar propagator (see Fig. 5.1 for particle labels), and $T_{N\alpha}$ is the isobar plane-wave amplitude as in Eq. (5.4).

To calculate spin observables one associates with each nucleon three orthogonal directions: N (normal), L (logitudinal), and S (sideways). N always means normal to the scattering plane as defined by the cross product of the beam direction and detected nucleon momentum; S lies in the scattering plane on the same side as the fully analysed particle ($\mathbf{S} = \mathbf{N} \times \mathbf{L}$), and L is the same as the beam direction.

We are interested in scattering situations when the spins of the initial

nucleons are polarized along one of these directions. Indicating with i and j the spin of the beam and the target, respectively, the five-fold polarized differential cross section will be abbreviated as

$$\sigma(i,j) \equiv \frac{d^5\sigma(i,j)}{dp_p d\Omega_p d\Omega_\pi} = K \sum_{m_1',m_2'} |\langle m_1', m_2' | T_{2\to 3} | i,j \rangle|^2 \qquad \text{(B.3)}$$

with K a constant (including phase space and flux factors) and $i,j = \pm N, \pm L, \pm S$ or 0 (when the nucleon is unpolarized).

Then, the beam asymmetries are defined as

$$A_{i0} = \frac{\sigma(i,0) - \sigma(-i,0)}{\sigma(i,0) + \sigma(-i,0)} \qquad \text{(B.4)}$$

and analogous expressions A_{0j} (the target asymmetry) with the beam unpolarized.

The initial state spin-spin correlations are

$$A_{ij} = \frac{\sigma(i,j) - \sigma(i,-j)}{\sigma(i,j) + \sigma(i,-j)}. \qquad \text{(B.5)}$$

The polarized cross sections which appear in the above formulas must then be expressed in terms of the matrix elements in Eq. (B.2). This can be easily done by noticing that the spin states needed to evaluate those matrix elements are

$$|\pm L\rangle \;=\; |\pm \frac{1}{2}\rangle$$

$$
\begin{aligned}
|\pm N\rangle &= \sqrt{\frac{1}{2}}(|+\frac{1}{2}\rangle \pm i|-\frac{1}{2}\rangle) \\
|\pm S\rangle &= \sqrt{\frac{1}{2}}(|+\frac{1}{2}\rangle \pm |-\frac{1}{2}\rangle).
\end{aligned} \tag{B.6}
$$

At this point, it is straightforward to express the amplitudes $\langle m_1', m_2'|T_{2\to 3}|i,j\rangle$ as a linear combination of matrix elements $\langle m_1', m_2'|T_{2\to 3}|\pm\frac{1}{2},\pm\frac{1}{2}\rangle$.

The vita has been removed from the scanned document